DEPARTMENT OF PHYSICS,
UNIVERSITY OF JYVÄSKYLÄ
RESEARCH REPORT No. 5/2013

NOVEL METHODS FOR ANALYSIS OF RADIOACTIVE SAMPLES USING POSITION-SENSITIVE DETECTORS, COINCIDENCE TECHNIQUES AND EVENT-MODE DATA ACQUISITION

by
JANI TURUNEN

Academic Dissertation
for the Degree of
Doctor of Philosophy

To be presented, by permission of the
Faculty of Mathematics and Natural Sciences
of the University of Jyväskylä,
for public examination in Auditorium FYS1 of the
University of Jyväskylä on May 23, 2013
at 12 o'clock noon

Jyväskylä, Finland
May 2013

ABSTRACT

Turunen, Jani
Novel methods for analysis of radioactive samples using position-sensitive detectors, coincidence techniques and event-mode data acquisition
Jyväskylä: University of Jyväskylä, 2013, viii + 63 p.
Department of Physics, University of Jyväskylä, Research Report 5/2013
ISBN 978-951-39-5197-9 (printed)
ISBN 978-951-39-5198-6 (electronic)
ISSN 0075-465X

A feasibility study on event-mode data acquisition systems, the alpha–gamma coincidence technique and position-sensitive detectors was conducted in Jyväskylä in the summer of 2007. Based on this study, a measurement device named PANDA (Particles And Non-Destructive Analysis) was designed and built at the Finnish Radiation and Nuclear Safety Authority (STUK). The PANDA device has two complementary measurement positions inside a vacuum chamber. The first measurement position hosts an HPGe detector for gamma and X-rays and a position-sensitive double-sided silicon strip detector (DSSSD) for alpha particles. The samples are analysed in close geometry between the detectors. The data are recorded in event mode and each event is time stamped. The second measurement position is equipped with a prototype silicon drift detector (SDD), which is used to detect conversion electrons and low-energy X-rays. The operation and performance of PANDA is presented via the measurements and analysis of various sample types. These include isolated radioactive particles, swipe samples, air filters and impactor samples. For example, the analysis of a cotton swipe sample containing 10 ng of Pu revealed that the $^{240}Pu/^{239}Pu$ atom ratio was 0.12 ± 0.03. The reference value given by the IAEA was 0.132. The results were congruent despite the fact that the sample itself was far from ideal. In another case, the alpha–gamma coincidence technique of PANDA was compared with traditional low-background gamma singles spectrometry. This comparison was realized by making long measurements in optimum geometries for a small radioactive particle. The analysis results proved that the alpha–gamma coincidence technique provide an approximately six times lower minimum detectable activity for ^{241}Am.

Keywords: non-destructive analysis, coincidence technique, event-mode data acquisition, position-sensitive detector, sample analysis

Author's address

Jani Turunen
STUK – Radiation and Nuclear Safety Authority
Finland
Address: Laippatie 4, FI-00881 Helsinki, Finland
email: jani.turunen@stuk.fi

Supervisors

Dr. Kari Peräjärvi
STUK – Radiation and Nuclear Safety Authority
Finland

Dr. Harri Toivonen
STUK – Radiation and Nuclear Safety Authority
Finland

Prof. Dr. Juha Äystö
Department of Physics
University of Jyväskylä
Finland
and
Helsinki Institute of Physics
Finland

Reviewers

Prof. Dr. Risto Orava
University of Helsinki
Finland

Dr. Stefaan Pommé
European Commission – Joint Research Centre –
Institute for Reference Materials and Measurements
Belgium

Opponent

Dr. R. Kurt Ungar
Radiation Protection Bureau
Canada

PREFACE

The majority of the studies reported in this thesis were done in the Security Technology laboratory of STUK during the years 2008−2012. The Security Technology laboratory was a part of the Research and Environmental Surveillance department.

I would like to express my gratitude here towards the people who have contributed to this thesis.

First of all, I would like to thank the Management of the Research and Environmental Surveillance department for giving me the opportunity and funding to carry out the work reported in this thesis.

Secondly, I would like to thank my supervisor Dr. Kari Peräjärvi. I am very grateful for his guidance through the years, starting back from the days when I did my master's degree. Without Kari's contribution this thesis would not have been made. I am also very grateful for the guidance of Dr. Harri Toivonen and Professor Juha Äystö who both have been my supervisors and given me valuable advice.

Since all the articles this thesis is based on have been group efforts, I would also like to thank each of the other authors and in particular Dr. Roy Pöllänen and Mr. Sakari Ihantola who have contributed to almost every one of the articles in some way. I would also like to thank all of my co-workers in the Security Technology laboratory. Through out the years they have given valuable support and provided an innovative working atmosphere. A special mention goes to Ms. Tarja Ilander for her work related to the data management of PANDA. I would also like to thank the Radionuclide Analytics laboratory for providing sources for the PANDA measurements.

I would also like to express my gratitude towards the following people: Mr. Ron Fox, Mr. Veikko Kämäräinen, Mr. Andreas Pelikan, Mr. Kari Salomäki, Dr. Heikki Sipilä and Mr. Asko Turunen. They have each contributed to the measurement setups of the PANDA device or to the analysis process of the data produced by PANDA.

Finally, I would like thank my wife Marika for her support and understanding during this long project and also Jere and Minea for keeping me occupied when not working with PANDAs.

Helsinki 30.4.2013
Jani Turunen

FIGURES

CONTENTS

1 INTRODUCTION

The Finnish Radiation and Nuclear Safety Authority (STUK) deals with a wide range of safety and security issues concerning man-made and natural radiation. STUK's mission is to prevent and limit the harmful effects of radiation. Areas of operation in STUK include nuclear safety regulation, radiation practices regulation, research, environmental monitoring and emergency preparedness. The Security Technology laboratory (TTL) is a part of STUK's Department of Research and Environmental Surveillance. TTL studies and develops measurement techniques, analysis methods and data management tools for applications in safety, security and safeguards (3S).

Radioactive substances in the environment are monitored throughout the world by many national and international bodies. The radiation measurement techniques used in the 3S sector have remained essentially unchanged [1]. Some progress has obviously been made through the years, but the basic sample analysis process has typically been based on a single measurement performed with a single detector and a multichannel analyser. Since the goal is to obtain as reliable and accurate results in as short a time as possible, this approach does not always provide the best possible overall outcome. The situation could be improved by adapting techniques commonly used in basic research.

Along these lines, a feasibility study was carried out by TTL personnel together with researchers of the IGISOL group at the University of Jyväskylä in the summer of 2007. This study focused on position-sensitive alpha particle detectors, the alpha–gamma coincidence technique and event-mode data acquisition. Based on the outcome of this feasibility study, a four-year research programme entitled Non-Destructive Analysis (NDA) was established at STUK. The NDA project was officially launched in 2008.

The goal of the NDA project was to improve the whole sample analysis chain by introducing new non-destructive analysis techniques and methods for 3S. The aim of the project was also to improve STUK's emergency preparedness capability in situations that could be threatening or dangerous to society. More precisely, the scope of the project extended from initial sample collection to

final analysis of the measurement data, including data management through a database.

The main product of the NDA project was the PANDA (Particles And Non-Destructive Analysis) device, which also is the core of this thesis. The articles of this thesis concentrate on the technical description of the PANDA device and its performance in measurements and analysis of various kinds of radioactive samples. The main focus has been on improving the reliability and sensitivity of non-destructive analysis techniques for samples containing hard-to-detect alpha-decaying nuclides.

These alpha-decaying nuclides are very important in the field of 3S. They are highly radiotoxic if inhaled or ingested [2], [3], some of them (U, Pu) can be used in nuclear weapons [4] and all of them in dirty bombs [5], [6]. For example, the former Russian agent Alexander Litvinenko was murdered in 2006 using radioactive ^{210}Po [7], [8]. Litvinenko suddenly fell ill and was hospitalised, and only three weeks later he died of radioactive poisoning. Radiological dispersal devices or dirty bombs are explosive devices that contain radioactive material. The actual health effects caused by the detonation of such a device would in most cases be small. The main effects would be economic and social, arising from the costs of cleanup in the area and the fear of radiation among the population [5]. Despite a global effort to ban nuclear weapons, the threat still remains, as countries like North Korea and Iran are advancing with their nuclear test and development programmes. The latest nuclear test was carried out by North Korea in February 2013. Reliable and rapid determination of Pu isotopes that can be used to produce nuclear weapons is a very relevant matter concerning global security and safeguards.

One especially important detection and analysis method employed in the PANDA device is the alpha–gamma coincidence technique. The possibility of using conversion electron spectrometry to study these alpha-decaying isotopes has also been examined during the NDA project. This work will continue in the future.

This thesis is based on the following enclosed publications:

1. Peräjärvi, K., Hakala, J., Jokinen, A., Moore, I.D., Penttilä, H., Pöllänen, R., Saastamoinen, A., Toivonen, H., Turunen, J. & Äystö, J. 2009. Event Mode Data Acquisition for Characterization of Samples Containing Radioactive Particles. IEEE Transactions on Nuclear Science 56 (3), 1444-1447.

2. Turunen, J., Peräjärvi, K., Pöllänen, R., Toivonen, H. 2010. PANDA – A novel instrument for non-destructive sample analysis. Nuclear Instruments and Methods in Physics Research A 613, 177-183.

3. Turunen, J., Ihantola, S., Peräjärvi, K., Pöllänen, R., Toivonen, H. 2010. Novel spectrometric approach to non-destructive characterization of safeguards samples. ESARDA Bulletin 45, 23-28.

4. Peräjärvi, K.A., Ihantola, S., Pöllänen, R.C., Toivonen, H.I., Turunen, J.A. 2011. Determination of ^{235}U, ^{239}Pu, ^{240}Pu, and ^{241}Am in a nuclear bomb particle using a position-sensitive α-γ coincidence technique. Environmental Science and Technology 45 (4), 1528–1533.

5. Turunen, J., Ihantola, S., Peräjärvi, K., Pöllänen, R., Toivonen, H., Hrnecek, E. 2011. Collection and behaviour of radon progenies on thin Mylar foils. Radiation Measurements 46 (6-7), 631-634.

6. Turunen, J., Ihantola, S., Peräjärvi, K., Toivonen, H. 2012. Comprehensive radioassays of samples using the PANDA device. Nuclear Instruments and Methods in Physics Research A 678, 78-82.

The author participated in the construction of the measurement setup and in the experiments done with it during the feasibility study. These are reported in [Publication 1]. The author has been involved with the design and construction of the PANDA device from the start and has also been mainly responsible for the operation of the device. The author has performed or taken part in all of the measurements done with the PANDA device and reported in the articles and also in the additional measurements presented here. The author is the main writer of [Publications 2, 3, 5 and 6] and participated in the writing of [Publications 1 and 4]. The author has done the main parts of the data analysis of [Publications 2, 5 and 6] and participated in the data analysis of [Publications 3 and 4].

2 THEORY AND FEASIBILITY STUDY

2.1 Theory

2.1.1 Alpha decay

Several naturally occuring nuclides of transuranic elements decay through alpha emission. Alpha emission occurs because the long-range Coulomb repulsion effect becomes increasingly important for heavy nuclei [9]. The distruptive Coulomb force increases with size at a faster rate (Z^2) than does the specific short-range nuclear binding force (approximately A). The spontaneus emission of an alpha particle can be represented as follows:

$$ {}^{A}_{Z}P_N \rightarrow {}^{A-4}_{Z-2}D_{N-2} + \alpha , \qquad (1) $$

where P is the parent nucleus, D the daughter nucleus, α a ${}^{4}_{2}He_2$ nucleus, A the mass number, Z the atomic number and N the neutron number.

The alpha particle has a very stable and tightly bound structure and it can therefore be emitted spontaneously. Energy must be released in order for the spontaneous decay to take place. In heavy nuclei, the alpha particle is emitted in preference to lighter particles, for which the decay would require an input of energy [10].

The energy released in alpha decay (Q_α) is given by the difference in mass energy between the parent nucleus and the final products. The Q_α value is also equal to the kinetic energy of the final products. It can be written as:

$$ Q_\alpha = (m_P - m_D - m_\alpha)c^2 = E_D + E_\alpha , \qquad (2) $$

where m_P, m_D and m_α are the masses of the parent, daughter and the alpha particle, and E_D and E_α are the kinetic energies of the daughter and the alpha particle.

Assuming that the parent nucleus is at rest, the conservation of linear momentum requires that the daughter nucleus and the alpha particle recoil in opposite directions with the same momentum, i.e., $m_D v_D = m_\alpha v_\alpha$, where v_D and v_α are the velocities of the daughter nucleus and the alpha particle. Therefore, the energy of the alpha particle can be written as:

$$E_\alpha = \frac{E_D \cdot m_D}{m_\alpha} = \frac{Q_\alpha}{1 + \frac{m_\alpha}{m_D}}. \qquad (3)$$

Typically, an alpha particle carries about 98% of the Q_α value and the much heavier daughter nucleus only about 2% [9]. The kinetic energies of alpha particles are typically about 4–10 MeV.

Due to the Coulomb barrier, nuclides that have large Q_α values have short alpha decay half-lives, while nuclides that have small Q_α values have long half-lives. For example, the half-lives ($T_{1/2}$) and Q_α values (ground state) of ^{239}Pu and ^{240}Pu are $T_{1/2}$ = 24110 a; Q_α = 5.244 MeV and $T_{1/2}$ = 6561 a; Q_α = 5.256 MeV, respectively, whereas the same values for naturally occurring radon progenies ^{212}Po and ^{214}Po are $T_{1/2}$ = 0.299 µs; Q_α = 8.954 MeV and $T_{1/2}$ = 164.3 µs; Q_α = 7.833 MeV, respectively [11]. All of these nuclides are 100% alpha emitters. These figures illustrate the sensitive relationship between the Q_α value and the barrier penetration probability.

2.1.2 Gamma decay of excited states

A very significant feature of alpha decay is that a given initial state can populate many different final states in the daughter nucleus. In general, heavier nuclides have a higher level density, but due to the nature of alpha decay, it primarily populates states at low excitation energies. The excited states decay through gamma-ray transitions or internal conversion [12].

In gamma decay, the different excited states rapidly decay to the ground state by emitting one or several gamma rays. Gamma-ray energies generally range from 20 to 200 keV. Gamma decay and also internal conversion lifetimes are typically very short, usually less than 10^{-9} s. States that have longer, measureable half-lives are called metastable or isomeric states, and their transitions are known as isomeric transitions [10].

The decay schemes or energy level diagrams for three nuclides relevant to this thesis, ^{239}Pu, ^{240}Pu and ^{241}Am, are presented in Appendix 1. For ^{239}Pu and ^{241}Am, these schemes are partial and show only the main transitions. The decay schemes are taken from from the recommended data website by the Decay Data Evaluation Project [13].

2.1.3 Internal conversion of excited states

Internal conversion is an electromagnetic process that competes with gamma-ray emission. Instead of emitting a photon, the electromagnetic fields of the nucleus interact with the atomic electrons, causing one of the shell electrons to be emitted from the atom [9]. In this process, an atomic electron takes up the energy released in the decay and is exited from its initial state to an empty state. If the energy released is greater than the binding energy of the electron, as is usually the case, the electron is ejected from the atom [12].

The kinetic energy (E_e) of the emitted electron in this case appears as the difference between the transition energy (ΔE) and the binding energy (B) that must be supplied to release the electron from its atomic shell.

$$E_e = \Delta E - B \tag{4}$$

For a given transition ΔE, internal conversion electrons will be emitted with different energies, since the electron-binding energy varies in different atomic orbitals. The resulting conversion electron spectra, even from a nuclide with a single gamma-ray emission, are composed of multiple discrete components that are seen as peaks [9].

Conversion electrons are labelled according to the electronic shell from which they come (K, L, M,...). These correspond to principal atomic quantum numbers (n = 1, 2, 3,...). The shells have atomic orbitals, leading to a substructure that can be seen if the resolution of the spectrometer is high enough. The subshells are typically denoted with a number after the main shell. For example, electrons from the subshells of the L shell are called L_I, L_{II} and L_{III} (or L1, L2 and L3) conversion electrons.

The internal conversion coefficient (α_{ICC}) tells the probability of conversion electron emission relative to gamma-ray emission for a specific transition. The α_{ICC} value can be calculated for the entire transition or for individual atomic shells, or even their subshells. In some cases, internal conversion can be dominant over gamma-ray emission, while in others it can be negligible [9].

Several factors contribute to the probability of internal conversion. The relative intensities can be compared for electric (E) and magnetic (M) multipoles with the following equations [9]:

$$\alpha_{ICC}(EL) \propto \frac{Z^3}{n^3}\left(\frac{L}{L+1}\right)\left(\frac{1}{\Delta E}\right)^{L+5/2} \quad (5)$$

$$\alpha_{ICC}(ML) \propto \frac{Z^3}{n^3}\left(\frac{1}{\Delta E}\right)^{L+3/2} \quad (6)$$

Examining these equations, one can see that the conversion coefficients increase for heavy nuclei with a dependence relative to Z^3. On the other hand, when the transition energies increase, the probability of conversion decreases. The multipole order (L) and the atomic shell number (n) also contribute to the conversion coefficient.

2.1.4 Characteristic X-rays

In the internal conversion process, the atom is left with a vacancy in one of the electronic shells. Electrons from higher shells rapidly fill this vacancy. This is accompanied by the emission of characteristic X-rays [9]. The energy of the X-ray is the difference between the vacant energy level and the energy level the electron comes from. The energies of characteristic X-rays are typically low (in the present work from a few keV to tens of keV). Characteristic X-rays can be used to determine the element in question, but they do not reveal nuclide-specific information.

An alternative process to the characteristic X-ray is the emission of an Auger electron. In this process, the energy of the relocating electron is transmitted to another electron, which then escapes the atom as an Auger electron [14].

2.1.5 Charged particle and photon interactions in matter

Different radiation types interact differently with matter. Because of this, various detectors are used to detect, for example, alpha particles and gamma rays. The properties of a sample also limit the radiation types that can be measured from it.

A heavy charged particle, such as an alpha particle, thermalizes in a very thin layer of material, as it loses its energy to atoms of the matter it passes through. During the slowing down process, the heavy particle moves in an almost straight line, since it is deflected very little by the Coulomb interactions with the electrons. Fluctuations in its energy loss are averaged out and the charged particle will have a definite range. This depends on its energy, mass, charge and also the nature of the stopping medium [10].

For photons there are three primary processes in which a gamma ray or X-ray interacts with matter. These are the photoelectric effect, Compton scattering

and pair production. The relative importance of each varies according to the energy.

At low energies, photoelectric absorption dominates. In photoelectric absorption, a photon loses all of its energy, as this is converted into releasing an atomic electron. The released photoelectron receives kinetic energy, which is the photon energy minus the binding energy of the electron. The atom may de-exite by releasing other less tightly bound electrons, or alternatively the vacancy in an inner shell may be filled by an electron from a higher shell, also causing the emission of a characteristic X-ray [10].

In Compton scattering, a photon with initial energy scatters from an electron. Part of the photon energy is transferred to the kinetic energy of the electron. The amount of energy the electron receives is dependent on the scattering angle. Compton scattering becomes the dominant interaction process in medium heavy materials when the photon energies reach a few hundred keV.

In pair production, the entire energy of the photon is converted into the creation of an electron–positron pair. Pair production is possible only for photon energies over 1.022 MeV, and the process becomes important when the energy of the photon exceeds several MeVs.

2.2 Alpha–gamma coincidence feasibility study

As discussed in section 2.1, alpha decay mainly populates states of the daughter nuclide at low excitation energies. Low-energy gamma rays and conversion electrons are often emitted in coincidence with the alpha particles. Since photoelectric absorption dominates at low energies, the resulting alpha-gated gamma-ray spectra can be nearly free from background caused by Compton scattering. This enhances the peak-to-background ratio if compared to a singles gamma-ray spectrum. The good peak-to-background ratio improves the accuracy of activity determinations. In addition, spectrum analysis becomes more straightforward with the condition that the detected gamma-rays are recorded in coincidence with alpha particles, since all peaks belong to alpha-decaying nuclides.

Event-mode data acquisition means that each single event registered by the detector is recorded separately and time stamped. It provides the possibility to carry out software-based coincidence spectrometry, among other useful features. The optimum spectrum for the final analysis can be generated after the measurement has finished.

When studying large-area samples, position-sensitive detectors can provide useful information on sample properties. For example, they can be used to screen samples, locate particles from them and even to compare different particles within a sample with each other. In contrast, a conventional silicon detector cannot distinguish radioactive material evenly spread in a bulk sample from a single particle or particles.

To test the ideas described above, a feasibility study was performed in the summer of 2007. The measurement setup was constructed in the IGISOL measurement area at the Accelerator Laboratory of the University of Jyväskylä (JYFL) (see Fig. 1). The setup was constructed inside a vacuum chamber and it consisted of a high-purity germanium detector (HPGe) and a doudle-sided silicon strip detector (DSSSD). The planar HPGe detector model was LEGe (Low Energy Germanium) and it was manufactured by Canberra. Its crystal had a diameter of 36 mm and a thickness of 15 mm. The DSSSD was obtained from Micron Semiconductor and its model was W1. The DSSSD had 16 front and 16 back strips forming a grid of 256 pixels. The pixel size was 3 mm * 3 mm. The data were recorded in event mode with a VME-based data acquisition system. The trigger signal was a logical OR between the detectors.

FIGURE 1. Measurement setup used in the feasibility study. The system was constructed in the IGISOL measurement area.

The test samples used in the feasibilty study were a radioactive particle originating from a nuclear bomb and air samples containing radon progenies collected on filters. The nuclear bomb particle was isolated from a soil sample collected near Thule, Greenland, where a US Air Force B-52 bomber carrying

four hydrogen bombs crashed in 1968 [15]. Hereafter in this thesis, the sample is simply referred to as the Thule particle. The air samples were collected in a small room located in the basement of the JYFL facility using a Lilliput air sampler from Senya Oy. A photograph of the Lilliput device in the sample collection site is presented in Figure 2.

FIGURE 2. Lilliput air sampler at the sampling site.

The samples were measured in a relatively close measurement geometry. This was made as tight as was easily achivable with the equipment available at the time. Measuring samples in a tight geometry using large area detectors provided a good overall detection efficiency. This is important, especially when making coincidence spectrometry, since the efficiency related to the coincidence events is equal to the product of the single detection efficiencies of the detectors. The downside of the tight measurement geometry is that it can lead to the summation of multiple events (X-ray+X-ray, X-ray+gamma ray, etc.), which is seen as spurious peaks in the produced spectra.

The source-to-detector distances (sdd) were approximately 7 mm for the DSSSD and 10 mm for the HPGe. Additional measurements where the DSSSD sdd was 35 mm were carried out to test what kind of hitmap the detector provided when the distance was longer. Photographs of the measurement geometries are presented in Figures 3a–d.

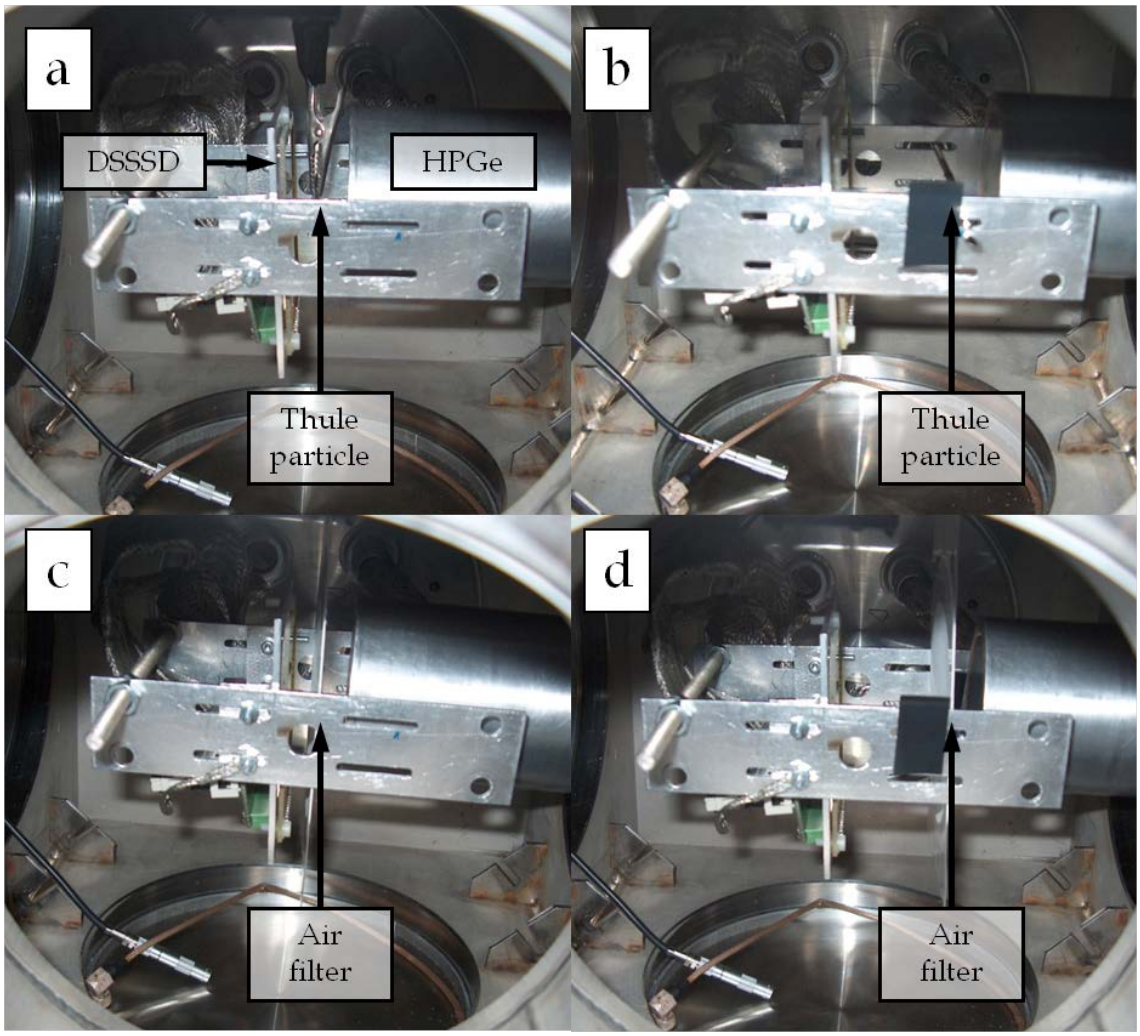

FIGURE 3. Feasibility study detector setup with different measurement geometries and samples. a) Thule particle, sdd(DSSSD) = 7 mm, sdd(HPGe) = 10 mm; b) Thule particle, sdd(DSSSD) = 35 mm, sdd(HPGe) = 10 mm; c) air filter, sdd(DSSSD) = 7 mm, sdd(HPGe) = 10 mm; d) air filter, sdd(DSSSD) = 35 mm, sdd(HPGe) = 10 mm.

The simultaneous measurement of alpha particles and gamma-rays and the use of an event-mode data acquisition system enabled software-based coincidence spectrometry to be performed. By setting a gate that takes into account only the alpha particle events in a desired energy region, and then gating the HPGe detector data with it, an almost background-free gamma-ray spectrum was provided. For example, Figure 4 presents the singles gamma-ray and the alpha-gated gamma-ray spectra. In addition to these, a spectrum from a background measurement is presented. The presence of ^{241}Am (peak at 59.5 keV) in the sample can be seen by comparing the singles gamma-ray spectrum with the background spectrum. However, the effect of alpha-gating results in a gamma-ray spectrum with negligible background and leads to a superior peak to background ratio if compared to the singles counting.

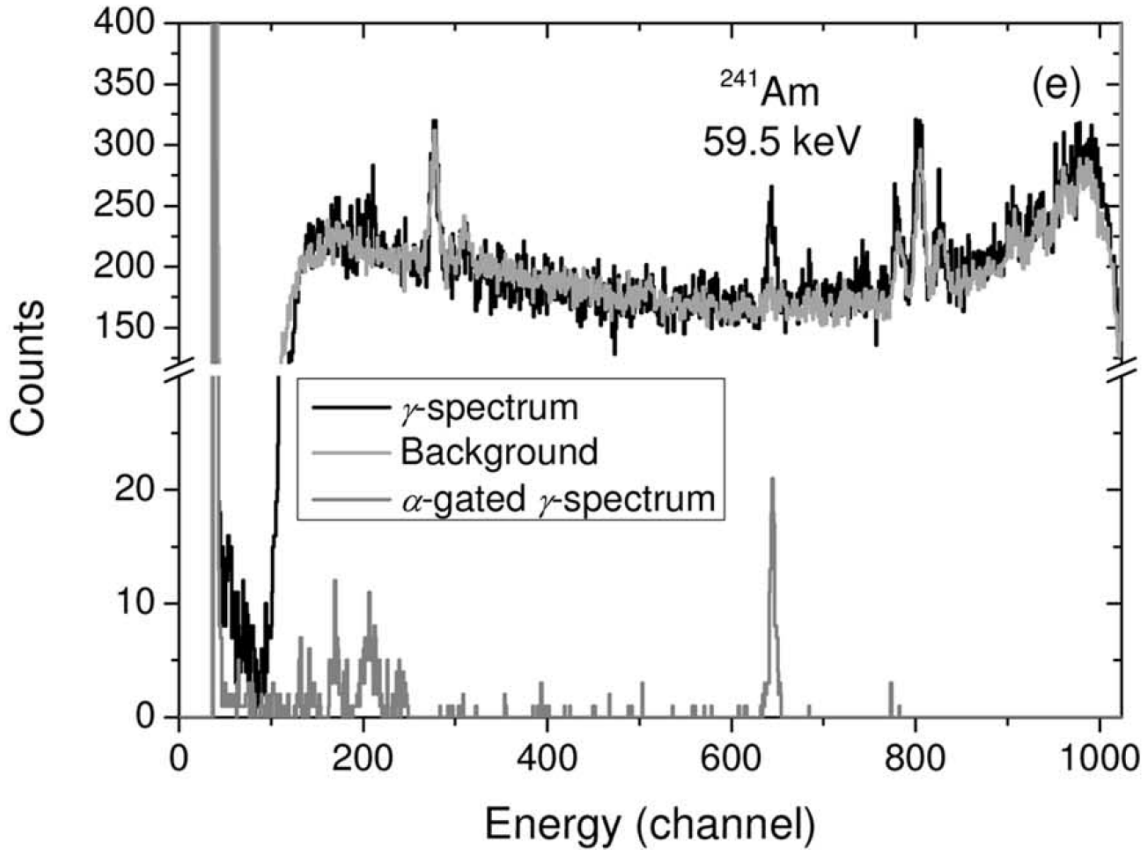

FIGURE 4. Singles and alpha-gated gamma-ray spectra measured from the Thule particle and the background spectra. The figure is taken from [Publication 1].

A position-sensitive alpha particle detector like the W1 used in the measurements can be applied to locate particles from large-area samples, such as air filters or swipes. Figure 5 presents a comparison of two 1 h measurements of the Thule particle where the source-to-detector distances were 35 mm and 7 mm. From Figure 5a it is impossible to determine how many radioactive particles cause the shape of the hitmap, since the detector is too far from the source. On the other hand, when the sdd is 7 mm, a distinctive peak shape becomes clear (see Fig. 5b). When attempting to locate particles, it is crucial that the sdd is set to a minimum.

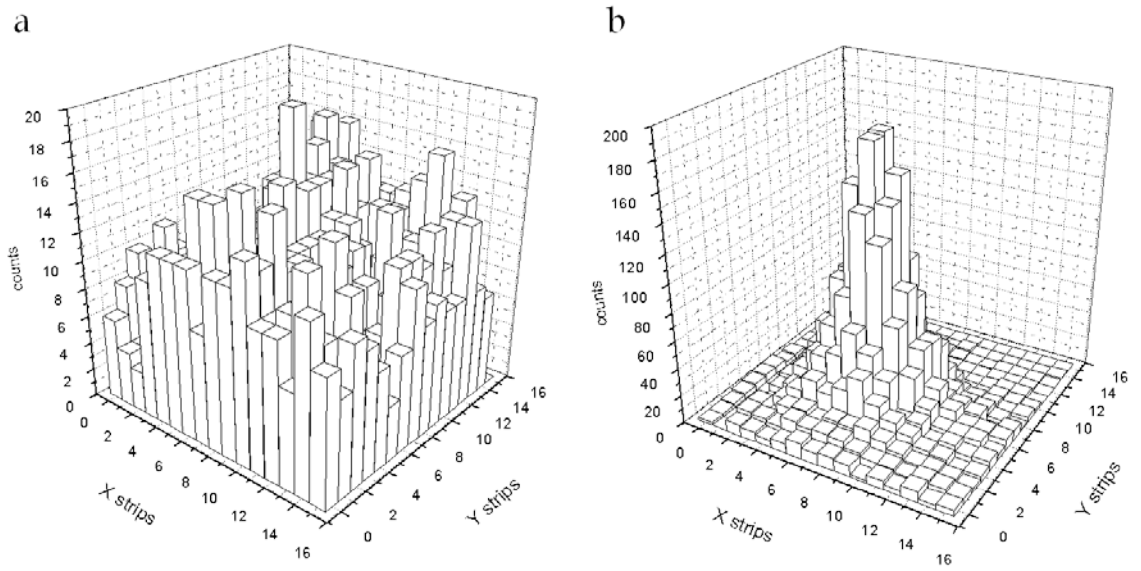

FIGURE 5. Two hitmaps created using the position-sensitive alpha detector. In both cases, the measured sample was the Thule particle. a) sdd = 35 mm b) sdd = 7 mm.

For an air filter, the collected airborne radon progenies are distributed evenly, causing the hitmap shape to be rather flat, no matter what the sdd is (for example, see Fig. 2 in [Publication 1]). Note that when screening large area samples, the background related to a single pixel is only a small portion of the background related to the whole detector (in this case 1/256). Since the majority of the events from a single radioactive particle are recorded with only a few pixels (see Fig. 5b), the overall effect caused by the background counts also becomes much smaller.

In addition, the alpha particle energy region of natural background caused by radon progenies is higher (over 6 MeV) than the energy region of relevant U and Pu isotopes (between 4 and 6 MeV). When using event-mode data acquisition, the main part of the natural background can be discarded from the final alpha-gated gamma-ray spectra by simply choosing an appropriate alpha gate in the analysis process.

The feasibility study proved that the capability for non-destructive analysis of samples containing radioactive substances could be significantly improved by applying the methods described above. Based on the knowledge gained, the NDA project was planned at the end of 2007 and launched at the beginning of 2008. The next step was to build a new measurement platfrom applying the techniques and methods tested and approved in the feasibility study. This was to be the PANDA device. The same nuclear bomb particle that was used in the feasibility study was later also measured with the PANDA device. The results of this study are presented in section 4.2.1.

3 PANDA

When designing the PANDA device, the goal was to make an instrument that could serve as a permanent setup in routine use and form a development platform on which new ideas and techniques could be tested. The technical design of PANDA's vacuum chambers and measurement setups were made by Kari Salomäki of engineering company Polartek Oy. The vacuum chambers along with other vacuum parts were constructed in the mechanical workshop of JYFL. The detectors, vacuum pumps, electronics and other parts were purchased from various commercial suppliers.

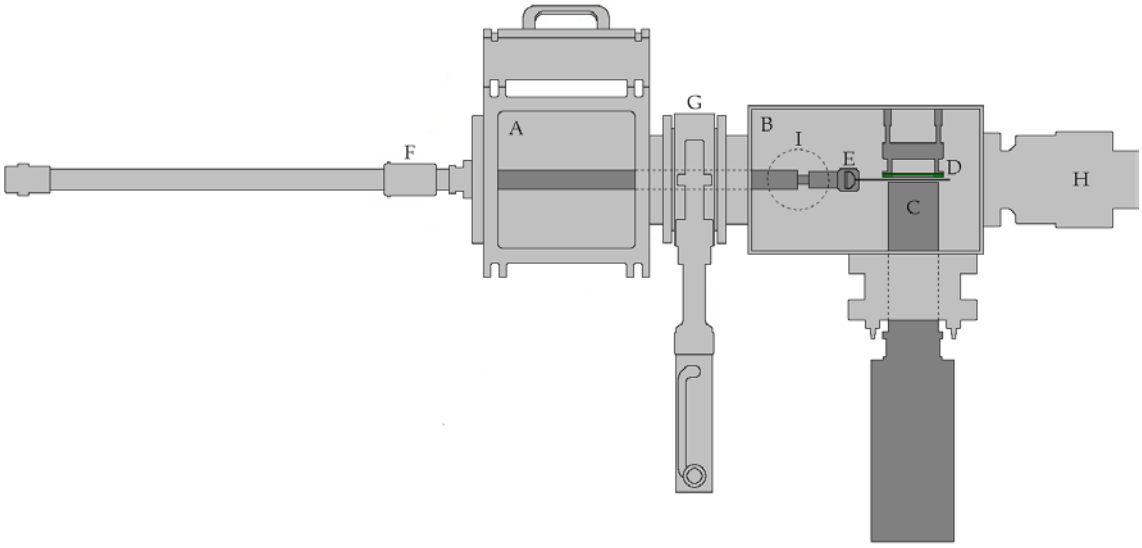

FIGURE 6. Schematic representation of the PANDA device. The view is from the top side. Explanation of letters: A = loading chamber, B = measurement chamber, C = BEGe detector, D = DSSSD, C+D = Measurement Position 1, E = sample holder, F = linear feedthrough, G = gate valve, H = turbomolecular pump, I = Measurement Position 2 (place marked with dashed line).

PANDA's core consists of two complementary measurement setups inside a vacuum chamber. The construction of the device began in early 2008 and the first test measurements were carried out in that summer. The first real sample measurements were performed in October 2008. The overall technical design and the operation of the first measurement position were published in [Publication 2]. Since then, upgrades and improvements have been made. The most notable of these is a second measurement position that was completed in 2011. The second measurement position along with other improvements were published in [Publication 6]. A schematical picture of the PANDA device is presented in Figure 6 and a photograph in Figure 7.

FIGURE 7. The PANDA device in March 2013.

3.1 General description of the PANDA device

The PANDA device has two vacuum chambers: a loading chamber and a measurement chamber (see Fig. 8). Both chambers are made of 6 mm thick steel. These chambers are connected to each other with a manually operated gate valve (VAT, series 12.1). The gate valve is used to isolate the chambers from each other. The loading chamber is intended for loading and changing samples. Its dimensions are 248 mm * 248 mm * 251 mm. The top flank opens up and the samples are installed from there. The measurement chamber's dimensions are 398 mm * 248 mm * 248 mm. With the gate valve closed, the measurement chamber can be kept in vacuum and its detector setups operational, even when changing samples. The measurement chamber has two locations for different measurement setups. However, only one of these so-called measurement positions, MP1 or MP2, can be used at a time. The same sample can be measured in both of them in turn if desired. The detector setups of MP1 and MP2 are discussed in sections 3.2 and 3.3.

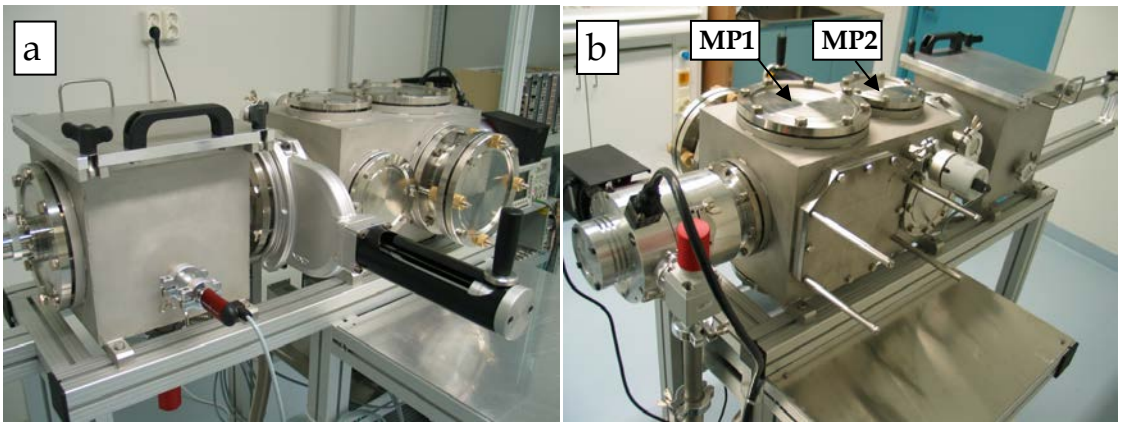

FIGURE 8. Front and rear views of the vacuum chambers of PANDA without the detector setups. a) The loading chamber (left) and the measurement chamber (right) are connected to each other with a manually operated gate valve. b) The octagonal flange in the side of MP1 is specially designed for a position-sensitive silicon detector setup (discussed in section 3.2.1).

The vacuum is created using two scroll pumps and a turbomolecular pump. The pumps are from Oerlikon Leybold Vacuum. The turbopump is a Turbovac 361, and according to its manual, it can in the best cases reach a vacuum that is under $1*10^{-10}$ mbar if UHV techniques such as copper gaskets are used. The oil-free scroll pumps are of the model Scrollvac SC 15 D, and they can reach a vacuum of $1.6*10^{-2}$ mbar. One of the scroll pumps is connected to the loading chamber and is only used after a new sample is installed inside

PANDA. The other is connected to the turbopump and is used as its prepump. The vacuum system of PANDA typically operates at approximately $5*10^{-6}$ mbar. In cases of very long measurements, a vacuum of $5*10^{-7}$ mbar can be achieved.

Precision valves from Pfeiffer Vacuum are used to control the pumping and the venting speeds of the chambers. This reduces the risk of contaminating the vacuum chambers, especially in the case of powder-like samples. The vacuum is monitored using a DualGauge measuring system from Pfeiffer Vacuum. It has two gauges: one connected to the loading chamber and the other to the measurement chamber.

The samples are installed on holders that consist of three aluminium plates and parts that bind these together. The inner plate is 0.5 mm thick and the two outer plates 1 mm thick. The function of the inner plate is to position the sample precisely and the outer plates lock the sample in place. These three are bound together from one side with two heel pieces and from the other with a copper spring mechanism. Sample holders (inner and outer plates) have been produced to fit different types of samples. A sample holder used with air filters is presented in Figure 9.

Before a sample is installed on a sample holder, it is usually covered with a thin Mylar foil from the side where the radioactive material is located. These foils are used to protect the detectors and the chambers from contamination. Typically a 0.5 µm thick Mylar foil is used.

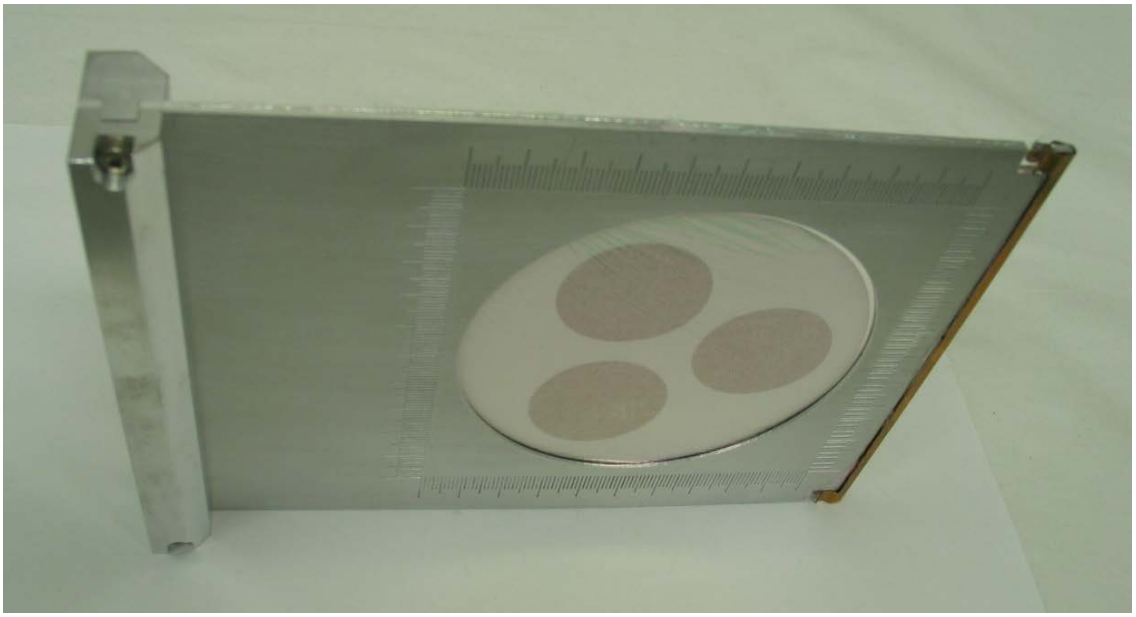

FIGURE 9. Sample holder with an air filter installed.

The sample holder is installed to the tip of a linear feedthrough inside the loading chamber. In the loading chamber there is also an alignment tool that is used to check that the sample holder is correctly installed. After the sample is loaded and the top flank closed, the loading chamber can be pumped to a

vacuum using the scroll pump. Since the scroll pump cannot reach as good a vacuum as the turbopump unit in the measurement chamber, the two vacuum chambers are also connected to each other with a stainless steel bellows that has a valve to control the air flow. This pipeline can be used to slowly balance the pressure difference before the gate valve is opened and the sample moved to the measurement chamber. The linear feedthrough is equipped with a precise scale that has an accuracy of 10 µm. Using the scale, the sample can be positioned accurately inside the measurement chamber.

3.2 Measurement Position 1

Measurement Position 1 (MP1) is intended for the screening and analysis of large-area samples such as air filters or swipes. It can also be used for other types of samples such as single radioactive particles or chemically prepared samples. The current measurement setup has remained unchanged since the first phase of construction of the PANDA device was initially completed. MP1 is capable of detecting gamma and X-rays and alpha particles.

3.2.1 Detectors

MP1 hosts a high-purity germanium detector (HPGe) and a double-sided silicon strip detector (DSSSD). The HPGe detector is from Canberra. Its type is Broad Energy Germanium (BEGe) and model BEGE3820. The crystal dimensions are 21 mm thickness and 70 mm diameter. The entrance window is made of carbon epoxy and its thickness is 0.5 mm. The distance from the window to the crystal is 5 mm. The BEGe detector can be used to measure gamma and X-rays from 3 keV to 3 MeV. The manufacturer's warranted and measured values for the detector resolution (full width at half maximum, FWHM) at different energies are presented in Table 1.

Table 1. FWHM values provided by Canberra for the BEGe detector at different energies.

Energy [keV]	FWHM [eV] warranty	FWHM [eV] measured
5.9	500	443
122	750	656
1332.5	2100	1850

In the measurements performed with PANDA, the BEGe is normally only used for the lower energies, since the interesting energy range usually ends at approximately 200 keV. The efficiency curve of the BEGe detector is illustrated

in Figure 10. For the efficiency calibration, a ^{133}Ba source was measured at a source-to-detector distance of 14.8 cm [Publication 4]. The shape of the efficiency curve was simulated using MCNPX (Monte Carlo N-Particle eXtended) [16]. The simulated curve was then scaled to fit the experimental data.

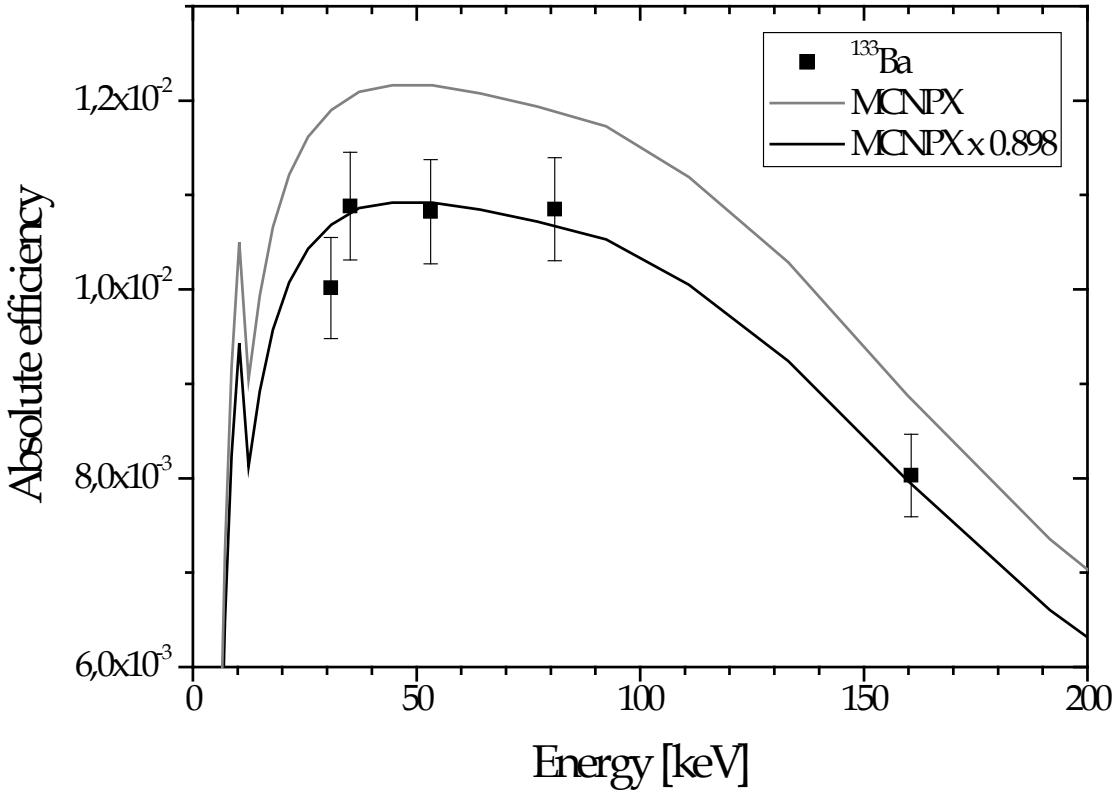

FIGURE 10. Absolute efficiency of the BEGe detector. The shape of the efficiency curve was obtained with MCNPX simulations and then scaled down to match the experimental ^{133}Ba data. The figure is modified from Figure 1 of [Publication 4]).

The endcap of the BEGe is modified so that it can be installed inside the measurement chamber (see Fig. 11). The endcap is longer than in standard versions and it has a welded flange that is used to connect the detector to an edge welded bellows. This bellows is then connected to the vacuum chamber and can be used to vary the position of the detector inside the chamber. In this way, the detector can be precisely placed in the desired position and the source-to-detector distance changed if necessary. The endcap is covered with a 6 µm thick Mylar foil to protect the detector from possible contamination.

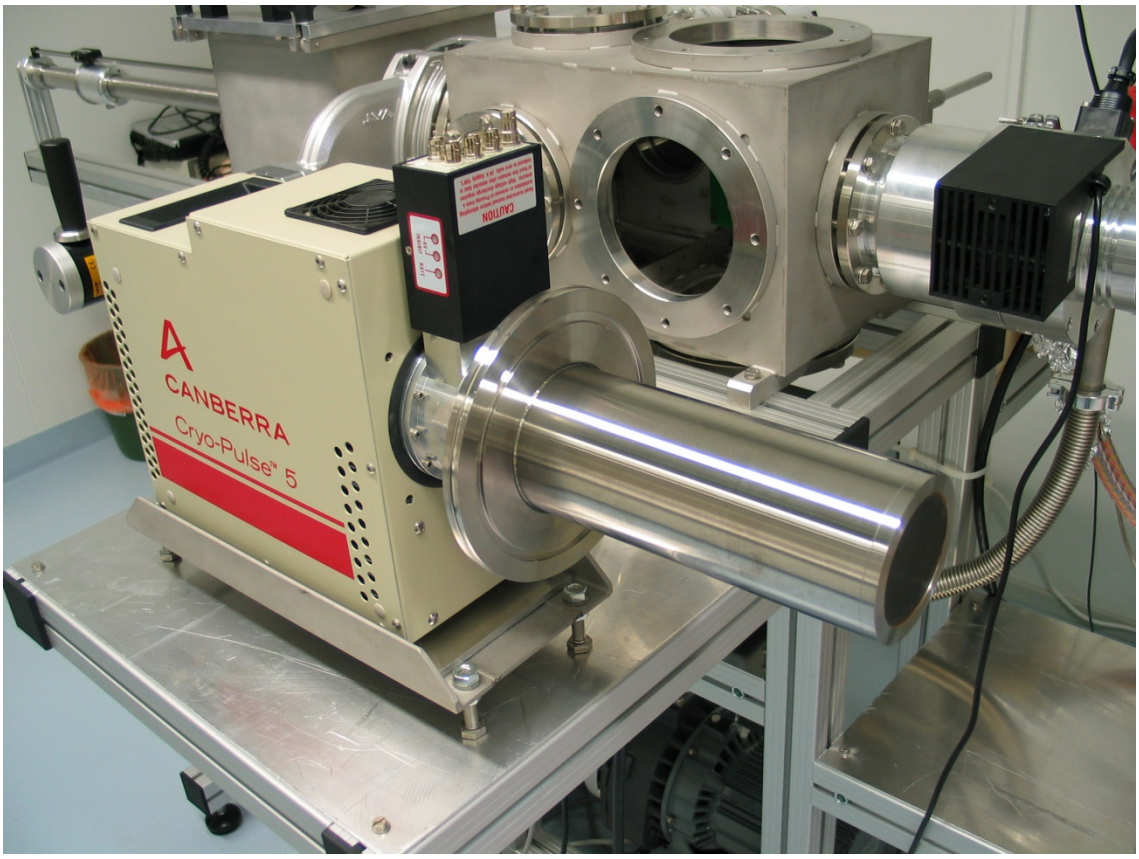

FIGURE 11. The BEGe detector of PANDA's MP1. The detector is installed inside the measurement chamber using the flange that is welded to the endcap. When the detector is installed to its place, there is an edge welded bellows assembly between the endcap's flange and the chamber. This bellows is used to adjust the distance of the detector inside the chamber.

The DSSSD is an alpha particle detector. Its model is BB7 from Micron Semiconductor. The thickness of the detector is 283 µm and its active area is 64 mm * 64 mm. It is composed of 32 vertical and 32 horizontal strips that are each 2 mm wide. On the front side of the detector the strips are vertical (X) and on the back side they are horizontal (Y). Each strip is used as a single detector, so the DSSSD has 64 detectors in total whose area is 2 mm * 64 mm each. When an alpha particle hits the detector, electrons are collected on the Y surface and holes to the X surface of the detector. Therefore, the front and back strips produce identical signals. When the recorded data is processed with appropriate software, these front and back strips form a grid of 1024 pixels. The position-sensitive DSSSD can be used to locate particles or to map the distribution of radioactive materials in large-area samples such as filters and swipes. The manufacturer's specifications state that the energy resolution of the detector for ^{241}Am alpha particles (E = 5.486 MeV) is typically 55 keV.

The DSSSD is installed on an aluminium holder that is connected to a specially designed octagonal flange (see Figs 8b and 12). The signals produced by the detector are transferred out of the chamber using four LEMO feedthroughs (16 channels each). The signal processing electronics are discussed

in the next section. The position of the DSSSD detector (orthogonal distance to the sample) can also be adjusted. This, however, has to be done outside the vacuum chamber by removing the whole detector setup and then lowering or raising the aluminium holder of the detector (see Fig. 12).

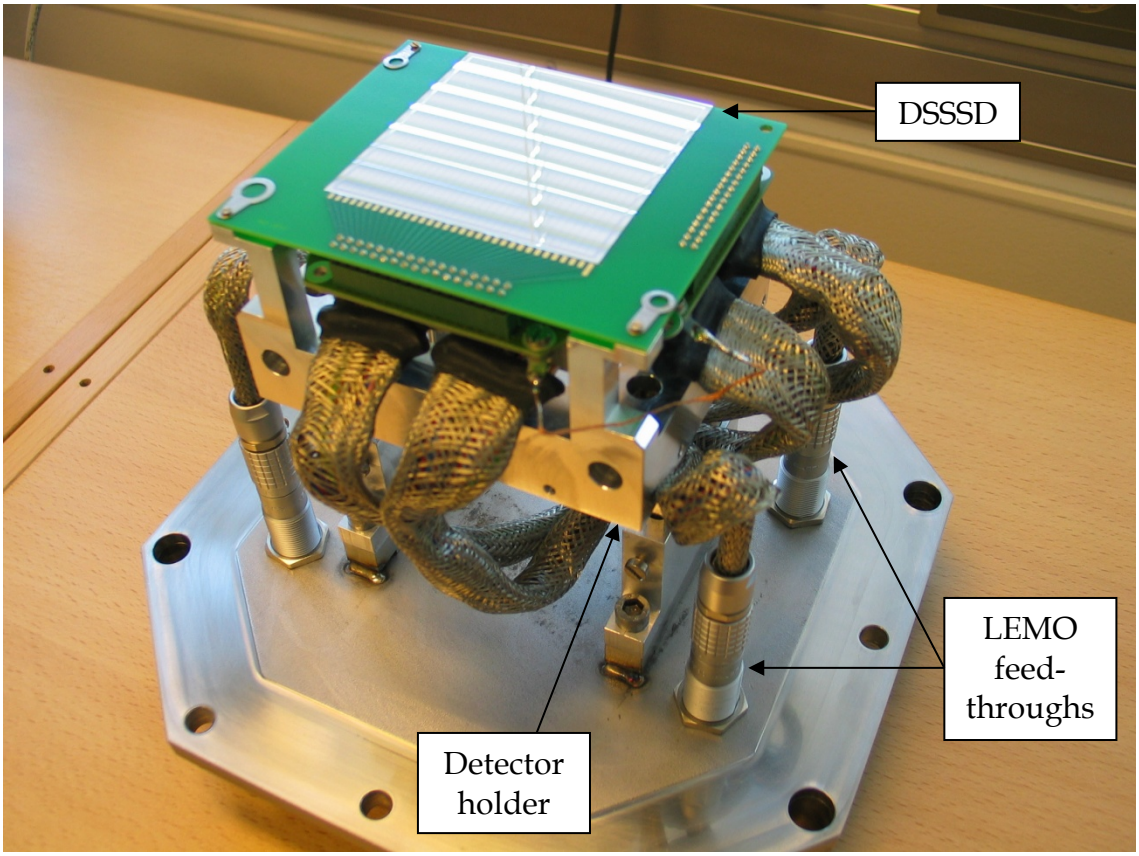

FIGURE 12. DSSSD detector installed on its holder. The holder is mounted on an octagonal flange.

The detectors of MP1 face each other and the distance between them is adjustable. This distance is usually 8 or 9 mm. The samples are transported with the linear feedthrough between the detectors and measured there (see Fig. 13). The source-to-detector distance is typically 3–5 mm, depending on the sample type.

On top of MP1 is a glass window that is used to view the measurement geometry. When a measurement is running, this window is covered with a plastic shield, since the biased Si detectors are sensitive to light. Above the window there is a video camera that is connected to a local TV screen and also to the data network of STUK. Using the camera and the view on the TV screen, the operator of the device can obtain visual confirmation of the sample position when inserting a sample in MP1. Simultaneously, the operator can confirm that the sample has survived the pump down without problems. The camera can also be used to document the measurement geometry by taking a snapshot with a web-based program.

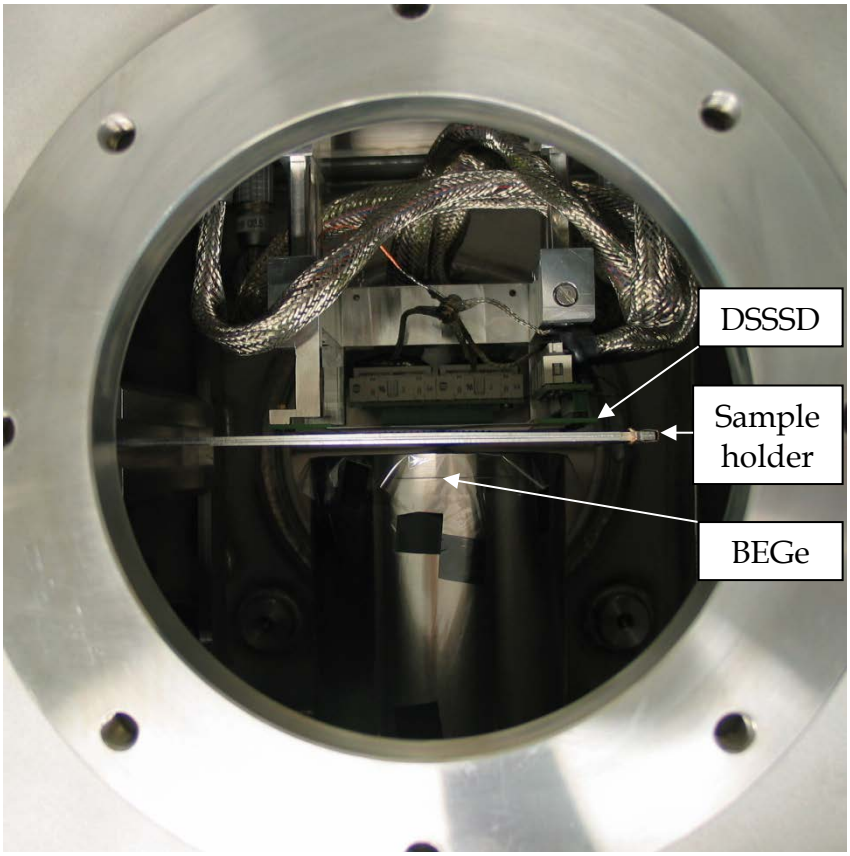

FIGURE 13. Top view of Measurement Position 1. The samples are measured between the BEGe detector and the DSSSD.

3.2.2 Electronics and data acquisition system

The electronics used to process the signals of the detectors in MP1 were presented in Figure 3 of [Publication 2]. Subsequently, some parts of the electronics have been modified. The current configuration of the signal processing electronics of MP1 is presented in Figure 14.

The signals from the DSSSD are processed using four MPRS-16 units from Mesytec. The MPRS-16 units have a preamplifier, a shaper (shaping time 1 µs), a timing filter amplifier and a leading edge discriminator in the same compact module. Each unit is able to process 16 channels, so two units are for the 32 front strips and two for the 32 back strips.

Each MPRS-16 provides a combined trigger signal. Earlier, all four triggers from the MPRS-16 units were used in the production of the final trigger signal. However, as discussed earlier, when an alpha particle hits the DSSSD, a front and a back strip register the event with identical energy, so the same information is produced twice. For this reason, the trigger signals are now only taken from the back strips.

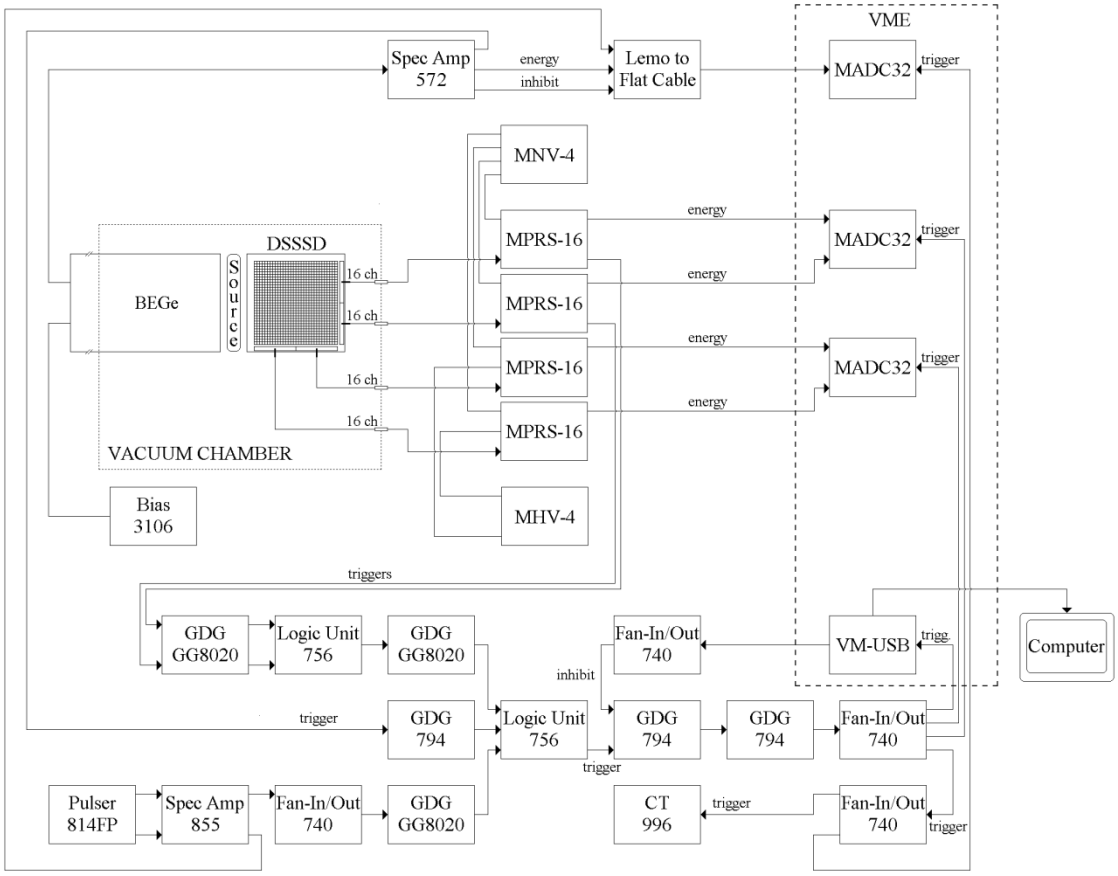

FIGURE 14. Electronics scheme for the signal processing and data acquisition of MP1. The scheme is modified from Fig. 3 of [Publication 2].

The energy signal from the BEGe preamplifier is processed with a model 572 amplifier from Ortec. The shaping time used is typically 1 µs. This amplifier was selected since it can be used to identify pulses caused by the summing of multiple low-energy gamma rays. The amplifier provides an inhibit signal when the energy signal is composed of multiple components. The efficiency of the circuit was experimentally determined to be approximately 5–10% [Publication 6]. This rough estimation was carried out by comparing the sum peaks from a spectrum created using the circuit with a spectrum where the circuit was not used. The data for these two spectra were recorded simultaneously. Like the energy signal, the inhibit signal is registered as a parameter with the data acquisition system and can therefore be used in gating the event data. The trigger signal of the BEGe is now also taken from the 572 unit.

The trigger signal of the BEGe detector is combined with the two trigger signals of the DSSSD along with a pulser signal. The pulser can be used for dead time determination (dead time determination can also be done with the data acquisition system). The final trigger signal is typically 1–2 µs wide. The

energy signals registered by the DSSSD come near the beginning of the gate and the signals from the BEGe near the end of the gate.

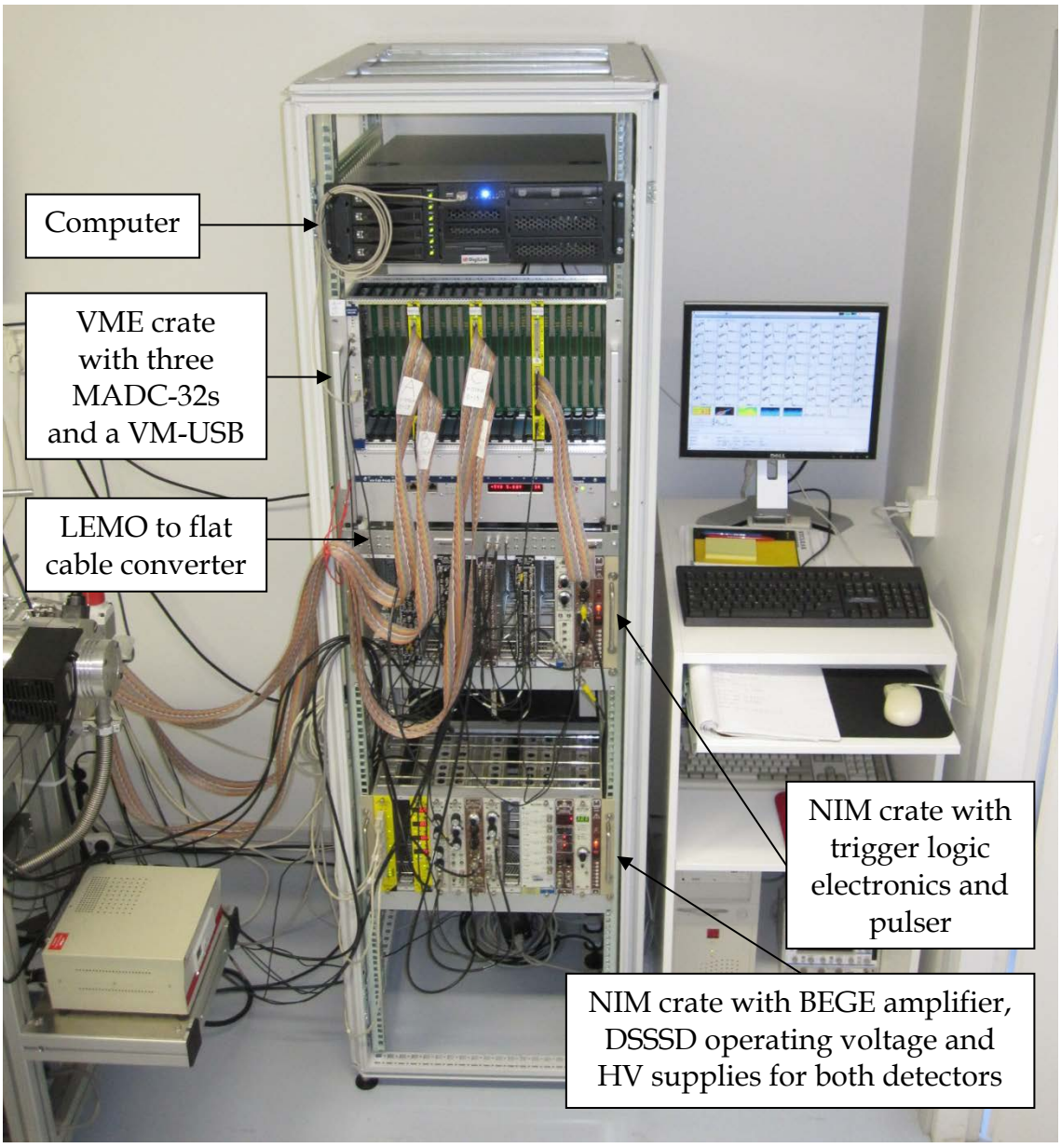

FIGURE 15. Electronics and data acquisition system of MP1.

The analogue to digital conversion of the energy signals and the pulser signal is carried out using three MADC-32 units from Mesytec, all of which are synchronized in time. The common clock rate is 16 MHz. This enables the correct build-up of events from the MADC-32 units. Events are time stamped with 1 µs accuracy. One MADC-32 is used for the 32 front strips of the DSSSD, the second for the 32 back strips and the third for the two signals from the BEGe detector and the pulser signal. In the third MADC-32 there are 29 free channels

that can be used when a new detector is added to the setup. A photo of the electronics and the DAQ computer is presented in Figure 15.

The event-mode data acquisition of MP1 is performed with a VM-USB-based data acquisition system that was developed and customized for the PANDA setup by Ron Fox of the National Superconducting Cyclotron Laboratory at Michigan State University [17].

The data acquisition system is controlled using a graphical user interface (GUI) (see Fig. 16). Besides stopping and starting measurements, the GUI can be used for creating spectra from the collected event data. Besides the singles spectra, for example, gated coincidence spectra, alpha particle hitmaps and the time behaviour of nuclides can be created. These spectra can be viewed on-line during the measurements and off-line after the measurements with a program called Xamine.

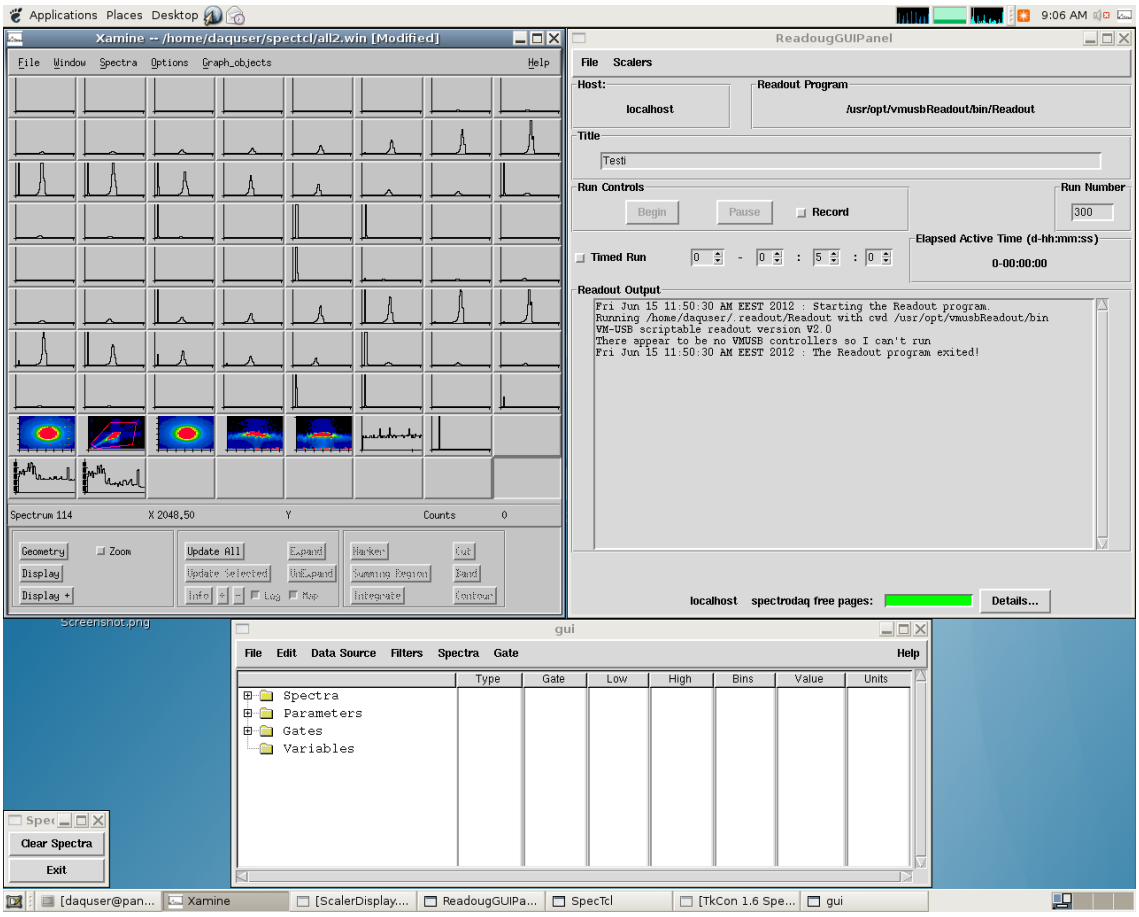

FIGURE 16. Screenshot of the control windows for the data acquisition system. The ReadoutGUIPanel on the top right is used for starting and stopping measurements. Using the GUI window on the bottom, the user can create various spectra. In the Xamine window at the top left, the user sees an on-line or off-line view of wanted spectra sorted from the recorded event data.

3.2.3 Data management and analysis tools

The binary event data along with additional metadata are converted to XML format and then stored in an extended LINSSI 2 database [18]. Since the overall data files can sometimes be very large, it is not reasonable to upload everything to the database. When uploading the data, certain restrictions can be applied. For example, if only alpha–gamma coincidence events are wanted, the single gamma ray and alpha particle events can be discarded. In this way, the processing of the data from the database for analysis becomes much quicker. The original binary data files are also always stored in the DAQ computer or an external hard drive for possible later use. The data management of MP1 is discussed in detail in [Publication 3].

Since the data are recorded in event-mode, the optimal spectra for the analysis process can be created after the measurements. The event data in the database can be sorted and viewed with a dedicated program called SPANDA (Software for PANDA). SPANDA was developed by Andreas Pelikan from Austria. The particle-locating algorithm used in SPANDA was developed by Sakari Ihantola of STUK.

SPANDA allows the user to analyse single measurement runs or to combine multiple runs of long measurements. Besides viewing singles spectra and alpha particle hitmaps created using the DSSSD data, the user can create coincidence spectra with the desired conditions set. For example, alpha-gated gamma-ray spectra can be generated using the total alpha events registered by the whole DSSSD or only a desired area of the DSSSD by marking the wanted pixels in the hitmap. The energy range of alpha particles used in the gating can also be adjusted to fit the needs.

When combining alpha spectra from the events recorded by multiple strips of the DSSSD detector, it is important that in each of these strips the gain value is as close to the others as possible. The gain cannot be separately set for each strip with the current hardware in use. This means that it has to be done afterwards with software. Therefore, one of the features of SPANDA is the gain-matching algorithm for the DSSSD strips. This enables the creation of better quality summed alpha spectra.

Another feature of SPANDA is the particle-locating algorithm. This algorithm uses the hitmap data of the DSSSD. With the particle-locating algorithm, the location of a single particle in a sample can be determined with a much greater accuracy than the pixel size of the detector. The function for automated particle locating has been tested with simulated data [19]. The simulations were performed for a single particle with a source-to-detector distance of 5 mm. When the number of counts registered by the DSSSD is small (less than 100), the particle location algorithm can give biased results. When the statistics improve, the algorithm provides more accurate results. With 1000 registered counts, the particle location is known with an accuracy of 0.42 mm in 68% of the cases. When the number of counts is increased to 10 000, the accuracy is 0.041 mm. These are for ideal cases.

Real samples can contain multiple particles, and this also has to be taken into account in the particle-locating algorithm. Having an estimate for the particle location is not enough. Also, how well the estimated location of the particle explains the measured hitmap needs to be known. This is done by studying χ^2 statistics of the fit with an automated function [19]. This function calculates the probability that the data given does not follow the expected form. The probability values of the χ^2 distribution can be used to estimate the quality of the fit. At first it is estimated whether the measured data can be explained with a single particle. The automated function first fits one particle to the measured hitmap and calculates the χ^2 value for the fit. After this, it fits two particles and again calculates the χ^2 value. If the first fit was better than the second one, the function prints the coordinates of the particle. If the second fit was better, the function adds a third particle and does the fitting and the comparison again. This goes on until the fit with fewer particles produces a better result.

After the optimal spectra have been created with SPANDA, spectral analysis can be carried out using various programs. Customized analysis software in use at STUK includes Aatami [20] and Adam [21]. The analysis results are also saved into the database and linked with the original measurement data. Many of the spectra published in the articles of this thesis were created and analysed using the general purpose OriginPro program [22].

3.2.4 Analysis of coincidence spectra

Usually, samples that contain ^{239}Pu and ^{240}Pu also contain ^{241}Am. Large amounts of Am can complicate the analysis, but Am can also be utilized in the analysis of the Pu isotopes.

The alpha–gamma efficiency ($\varepsilon_{\alpha\gamma}$) is a product of the alpha efficiency (ε_α) and the gamma efficiency (ε_γ). The alpha efficiency can usually be determined using the 59.5 keV peak of ^{241}Am in the alpha-gated and singles gamma-ray spectra [23]. The detection efficiency for the alphas from ^{241}Am can be calculated with the equation:

$$\varepsilon_\alpha = \frac{\varepsilon_{\alpha\gamma}}{\varepsilon_\gamma} = \frac{A_{\alpha\gamma}}{A_\gamma}, \qquad (7)$$

where $A_{\alpha\gamma}$ and A_γ are the areas of the 59.5 keV peaks in the alpha-gated and the singles gamma-ray spectrum, respectively. When deriving the equation, the activity of the sample (a), gamma-ray yield (b_γ) and measurement time (t) are cancelled out and the total alpha yield (b_α) is one for ^{241}Am.

This method applies when the 59.5 keV peak is clearly visible in both alpha-gated and singles gamma-ray spectra. The obtained value is typically also

a good approximation for other nuclides, such as ^{239}Pu and ^{240}Pu, that have alpha energies near ^{241}Am. The efficiency generally applies to any nuclides in the same geometry, if the sample matrix does not prevent the detection of emitted alpha particles. The alpha gate used in the initial analysis also needs to be broad enough. Before making a generalization of the determined alpha efficiency, one also needs to compare the DSSSD hitmaps made with different gating conditions [Publication 3].

The gamma efficiency can be determined in a similar way to the alpha efficiency in the case where the ^{241}Am area can be reliably determined from the singles alpha spectrum [23]. The peak detection efficiency for 59.5 keV gamma rays can be determined with the equation:

$$\varepsilon_\gamma = \frac{\varepsilon_{\gamma\alpha}}{\varepsilon_\alpha} = \frac{A_{\gamma\alpha}}{y_\gamma A_\alpha} = \frac{A_{\gamma\alpha}}{0.359 A_\alpha}, \tag{8}$$

where $A_{\gamma\alpha}$ and A_α are the areas of ^{241}Am in the 59.5 keV gamma-gated and the singles alpha spectrum, respectively, and $\varepsilon_{\gamma\alpha}$ is the gamma-alpha efficiency. The yield of the 59.5 keV gamma of ^{241}Am is 0.359.

The alpha–gamma efficiency can be determined for the 59.5 keV gamma rays by combining the two previous equations:

$$\varepsilon_{\alpha\gamma} = \varepsilon_\gamma \varepsilon_\alpha = \frac{A_{\alpha\gamma} A_{\gamma\alpha}}{0.359 A_\alpha A_\gamma}. \tag{9}$$

Note that $A_{\gamma\alpha} = A_{\alpha\gamma}$.

In many cases it is necessary to determine the shape of the ^{241}Am alpha spectrum by gating the total alpha spectrum with the 59.5 keV gamma rays. The resulting shape can also be used in the analysis of the entire singles alpha spectrum. Since the alpha energies of ^{239}Pu and ^{240}Pu are very close to each other, these isotopes cannot usually be separated using the alpha spectra. If the alpha efficiency is known, the sum activity of $^{239+240}$Pu can determined from the singles alpha spectra:

$$a_{Pu} = \frac{A_{\alpha,Pu}}{\varepsilon_\alpha t}, \tag{10}$$

where a_{Pu} is the sum activity of $^{239+240}$Pu and $A_{\alpha,Pu}$ the area of the $^{239+240}$Pu alpha peak [23].

When calculating the ^{240}Pu/^{239}Pu isotope ratio using alpha-gated gamma-ray spectra, the gamma efficiency curve must be known. Nuclides that have peaks near each other are rather insensitive to small uncertainties in the shape of the efficiency curve [23]. The relative efficiency calibration can be carried out with Monte Carlo simulations, and if the measured sample contains a lot of

^{241}Am, its gamma-ray peaks can be used to verify the simulation and to put it into an absolute scale [24].

Even the most intense gamma-ray transitions of ^{239}Pu and ^{240}Pu have small yields [11]: ^{239}Pu: E_γ = 38.661 keV, I_γ = 0.0104
E_γ = 51.624 keV, I_γ = 0.0272
^{240}Pu: E_γ = 45.244 keV, I_γ = 0.0447.

This means that the peaks in the alpha-gated gamma-ray spectra are typically very small and the peak fitting has to be done carefully. Each of the three Pu peaks lie in the energy region where the efficiency curve is relatively smooth, and the nearby ^{241}Am peaks can also be used to improve the efficiency calibration (see also Fig. 10).

If a large amount of ^{241}Am is present in the sample, the Pu peaks can be masked by the summing of low-energy X-rays and gamma rays. This effect can be diminished by using an absorber between the source and the BEGe detector [Publication 3]. The effect of the absorber has to be taken into account when performing the efficiency calibration [24]. These issues are discussed in section 4.

The individual activities of ^{239}Pu and ^{240}Pu can be determined from the alpha-gated gamma-ray spectrum or through the sum activity and the ^{240}Pu/^{239}Pu isotope ratio [23]. Analysis based on the alpha-gated gamma-ray spectrum requires the use of absolute alpha–gamma efficiency. For the latter option, the absolute alpha and relative gamma efficiencies are needed. Thus, if the summed Pu activity a_{Pu} and the ratio $r_{Pu} = a_{Pu-240} / a_{Pu-239}$ are known, the individual plutonium activities can be solved with the following equations:

$$a_{Pu-240} = \frac{r_{Pu} a_{Pu}}{1 + r_{Pu}} \tag{11}$$

$$a_{Pu-239} = \frac{a_{Pu}}{1 + r_{Pu}} \tag{12}$$

3.3 Measurement Position 2

Measurement Position 2 (MP2) is used for further analysis of interesting parts of the samples studied in MP1. It can also be used as an independent measurement setup for radioactive particle samples or chemically prepared samples.

In the initial design of PANDA, the second measurement position was taken into account. When MP1 was completed it was not yet entirely clear what MP2 would contain. A feasibility study was conducted in 2009 to map out suitable detectors. In the feasibility study, a few detectors used in JYFL were

tested, but the most suitable detector came from Oxford Instruments Analytical in Espoo.

3.3.1 Hardware

MP2 is equipped with a prototype silicon drift detector (SDD) (see Fig. 17). The active area of the SDD is 10 mm^2. There is a collimator made of gold in front of it. This reduces the area of the detector to 7 mm^2. The thickness of the detector is 450 µm. It can be used to detect electrons and X-rays down to energies of 1 keV. The useful range for X-rays ends at approximately 30 keV, since the detection efficiency rapidly drops at higher energies. The X-ray peaks can be used to reveal elemental properties. Conversion electron transitions are isotope specific, so the ability to perform conversion electron spectrometry provides an independent and complementary way to determine isotope ratios, such as $^{239}Pu/^{240}Pu$. Note that the low-energy transitions of actinides are often highly converted.

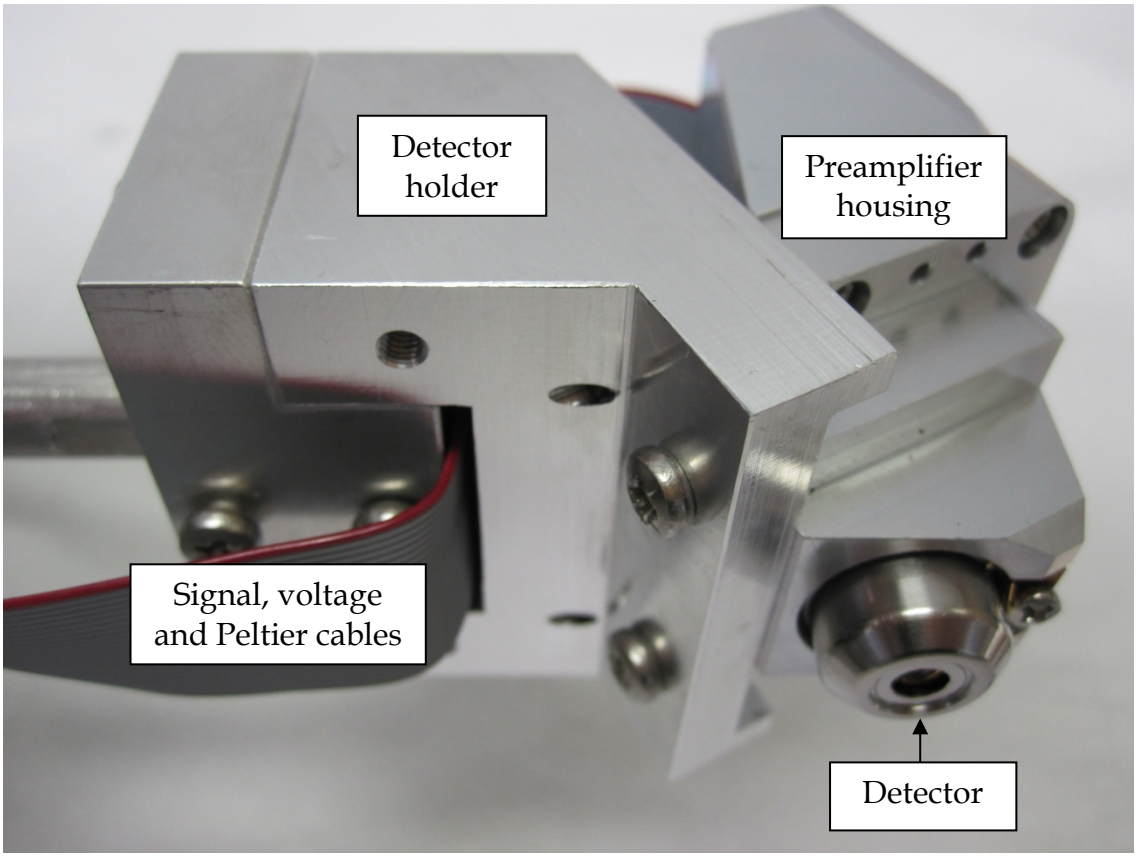

FIGURE 17. Silicon drift detector mounted on its holder.

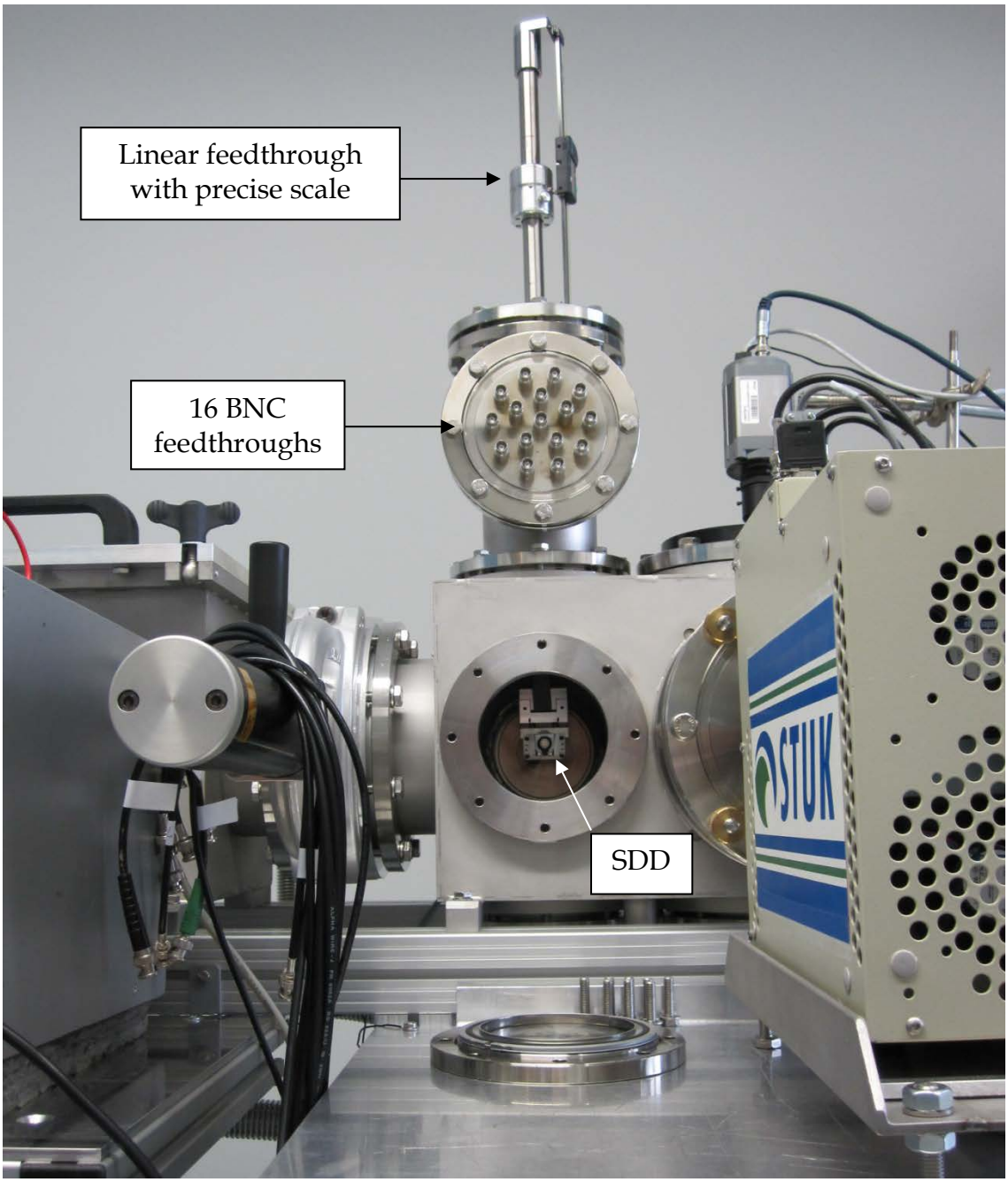

FIGURE 18. The SDD detector of MP2 in a typical measurement position. The blanking flange in front of it is removed. The vertically moving linear feedthrough on top of MP2 is used to lower the detector to the vicinity of the sample. The sample is transported to the measurement position with a horizontally moving linear feedthrough.

The preamplifier of the detector is installed right next to it. The detector is cooled with a Peltier element. The temperature is monitored with a thermistor connected to a multimeter. The current for the Peltier element along with operating and bias voltages to the detector preamplifier are supplied with conventional current and voltage sources. The current and voltages to the detector and the energy signal from the preamplifier to the amplifier are

transported via BNC feedthroughs (see Fig. 18). There are a total of 16 feedthroughs welded to a flange. Not all of these are needed for the SDD, and the supplementary feedthroughs are present in case a second detector is later added to MP2.

The SDD detector is installed on the tip of a linear feedthrough. This linear feedthrough is also equipped with a precise scale that has an accuracy of 10 μm. This feedthrough moves vertically inside the measurement chamber. Since the linear feedthrough that transports the samples to the measurement positions moves horizontally, these two feedthroughs can be used to position the SDD detector to face any part of a sample. After a large-area sample, such as a swipe or a filter, is screened in MP1 it can be moved to MP2 using the hitmap information provided by the DSSSD detector. The x- and y-coordinates obtained from the hitmap can be used to calculate the optimal settings for the feedthroughs, and thus position the sample optimally in MP2.

If an MP2 measurement is to be carried out for a radioactive particle or some other small-area sample whose location is precisely known, screening of the sample in MP1 is not needed. In this case, the sample can be transported directly to MP2.

3.3.2 Data management and analysis software

The data acquisition in MP2 is carried out using VASIKKA software developed at STUK by Tero Karhunen. The data are automatically saved to a LINSSI 2-based database in spectral format. The desired time interval can be set and a 40 s period is usually used.

The spectra can be viewed from the database with a program called LIBS, which was developed at STUK by Samu Ristkari. After forming the final spectra in LIBS, the user can automatically launch the analysis program AATAMI. The results of the analysis are saved to the same database. The final analysis methods for the spectral data of MP2 are out of the scope of this thesis. General purpose analysis software, known as AMUFI, is under development at STUK. The conversion electron peak shapes differ from those of gamma- and X-ray peaks, and their absolute yields are not always know with high enough accuracy.

4 OPERATION AND PERFORMANCE OF PANDA WITH VARIOUS SAMPLE TYPES

The PANDA device can be used to measure various types of radioactive samples, including radioactive particles, swipes, air filters and impactor samples. Since PANDA uses non-destructive methods, it does not harm the sample. Therefore, the same sample can be analyzed afterwards with other techniques if desired. Typically, the samples are measured as such. Only a thin protective foil, such as mylar, is used to cover the samples before measurement to protect the detectors and chambers from contamination. Radiochemically prepared samples can be also measured in PANDA. For the alpha–gamma coincidence technique, the samples need to be prepared on thin foils, i.e. no thick metal plates can be used.

Some restictions exist for the sample types that can optimally be analyzed with PANDA. One of them is the thickness of the sample. The sample material should be as thin as possible, because alpha particles and also low-energy gamma and X-rays can be absorbed in a thick sample. Since alpha particles deposit energy when they travel through material, including the sample matrix, the radioactive material should be as close to the sample surface facing the DSSSD as possible. With many nonmanipulated samples, the quality of the alpha spectra of MP1 is not very good, but this does not matter since the alpha particles detected with the DSSSD are primarily used to gate the BEGe data to produce alpha–gamma coincidence spectra. It is important that a good detection efficiency is obtained for both detectors, since the overall alpha–gamma efficiency is their product. The same restriction on sample thickness also applies for MP2, since only a very thin material layer is needed to stop conversion electrons.

Another sample restriction is the size. It is not easy to measure samples that are much larger than the active area of the DSSSD. If this is desired, the sample has to be measured in several parts.

4.1 Sample screening with MP1

Typically, a sample is first screened in MP1. The initial screening can last from a few minutes to a few hours or even overnight, depending of the activity of the sample. The results can be viewed on-line using the Xamine program. After the initial screening, sample measurement can be continued in MP1 if better counting statistics are required. The sample can also be moved to MP2 for further measurements.

In some cases, summing of X- and gamma rays can cause unwanted peaks in the alpha-gated gamma-ray spectra, which can lead to problems in the analysis process. The low-energy X-ray region can be removed from the measurement by placing an attenuator between the BEGe detector and the sample. A Ti foil was used to remove the sum peaks caused by ^{241}Am X-rays [Publication 3]. Such attenuators are usually implemented after the initial screening of the sample.

4.2 Detailed analysis of samples with MP1

The PANDA device has been used in measurements ranging from single radioactive particles to large bulk samples. Measurements carried out in MP1 for different sample types are summarized here. Most of these studies have been published in the articles of this thesis. Some additional information from the measurements is also incorporated.

4.2.1 Particle samples

Particle analysis has an important role, especially in the analysis of safeguards samples, where the properties of individual radioactive particles are more important than the bulk properties of the sample.

The first real sample measurement with the PANDA device was the study of the Thule particle used in the feasibility study at Jyväskylä. The particle was measured in MP1 for a total of three weeks. The detailed analysis of this sample is presented in [Publication 4]. The Thule article can also be viewed as a step-by-step description of how to perform sample analysis using PANDA's MP1.

Particles are located with the DSSSD alpha particle hitmap. The shape of the hitmap can provide information on the measured sample type, i.e. if the sample is a single small particle or if the radioactive material is spread over a larger area (see Fig. 3 of [Publication 4]). In this case, a measurement time of a few minutes would have been enough to verify that the sample is a single radioactive particle or at least that the radioactive material is concentrated in a very small area (see Fig. 19). For example, in three minutes the closest pixels to

the Thule particle register over ten alpha particles, whereas pixels further away basically register zero counts (Fig. 19b).

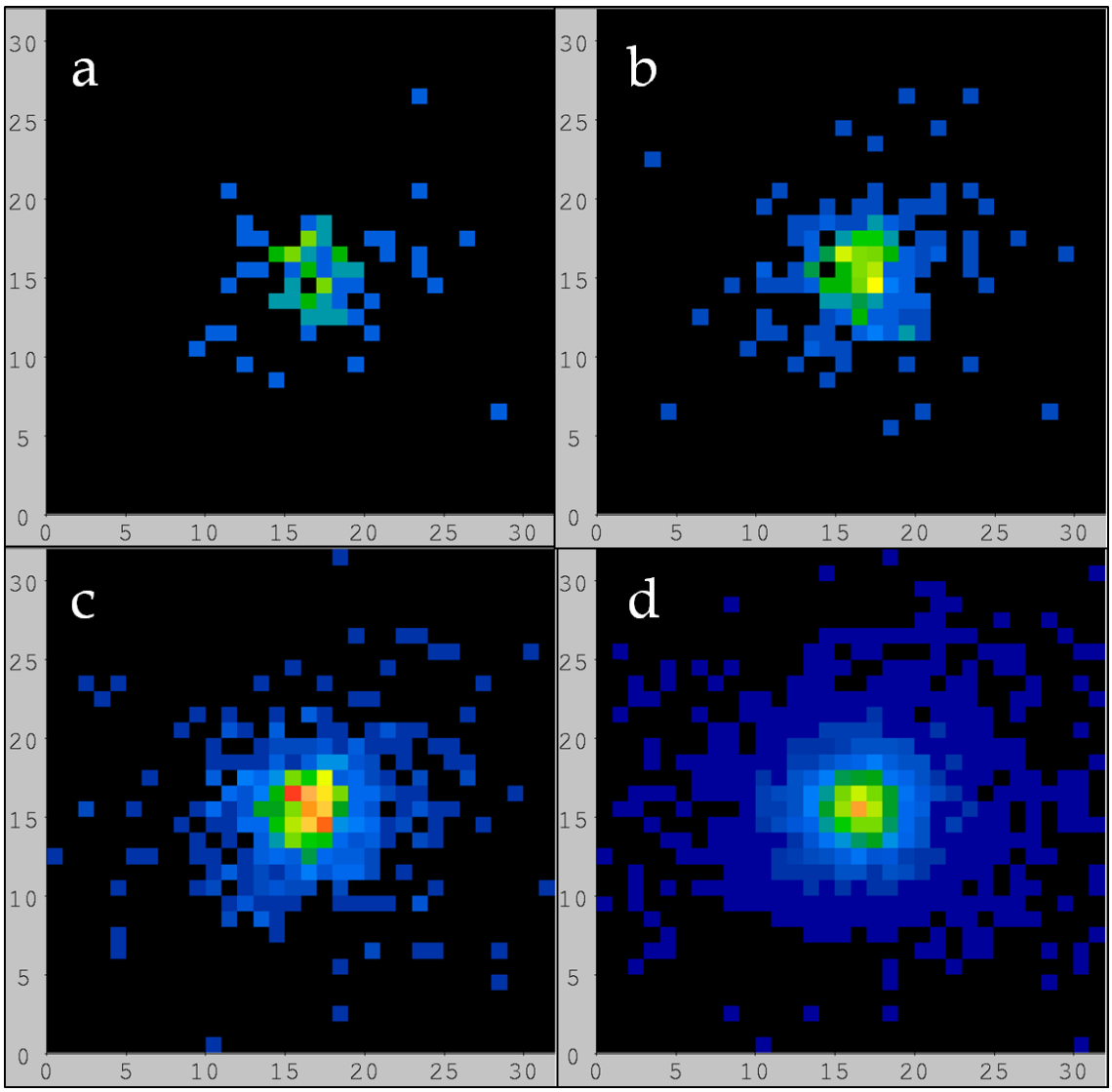

FIGURE 19. Alpha particle hitmaps registered with the DSSSD at the start of the Thule particle measurement. The data acquisition times were: a) 1 min b) 3 min c) 10 min d) 60 min.

Since alpha particles lose energy when they travel through material, the alpha spectra can also give valuable information on the size of the particle (assuming that we have an isolated particle). The smaller the particle is, the smaller is also the energy deposition into it. The Thule particle's diameter is a few tens of micrometres, so the quality of the alpha spectra is reasonable, but far from optimal (see Fig. 4 of [Publication 4]). The alpha spectra can give preliminary information on the nuclides present in the sample, but in many cases this information is insufficient. For example, solving the $^{240}Pu/^{239}Pu$ ratio using alpha spectra is impossible, since the alpha energies of these nuclides are

too close to each other (5156.6 keV for ^{239}Pu and 5168.2 keV for ^{240}Pu [11]). The alpha spectrum is also able to show the existence of ^{241}Am or ^{238}Pu (energies 5485.6 keV and 5499.0 keV, respectively [11]) in the sample.

Even the strongest ^{239}Pu and ^{240}Pu gamma-ray transitions (^{239}Pu E_γ = 38.661 keV and 51.624 keV; ^{240}Pu E_γ = 45.244 keV) are weak [11]. These Pu peaks are not visible in the singles gamma-ray spectrum presented in Figure 20. Only the presence of ^{241}Am and naturally occurring ^{210}Pb can be verified from the singles gamma-ray spectrum.

Creating a gamma-ray spectrum using only those gamma rays registered simultaneously with alpha particles is very important in determining the Pu isotope ratio. The alpha-gated gamma-ray spectrum of the Thule particle from the same energy region as the singles gamma-ray spectrum (Fig. 20) is presented in Figure 21. This spectrum illustrates that with the help of alpha gating, the low-yield Pu transitions become easily visible. Using the alpha–gamma coincidence technique, a ^{240}Pu/^{239}Pu atom ratio of 0.053 ± 0.011 was obtained [Publication 4]. This result is consistent with other analyses performed on similar samples using, for example, destructive methods such as mass spectrometry [25], [26].

Note that the background (spectrum baseline) in the PANDA singles gamma-ray spectra is larger than the background in the gamma laboratory of STUK. However, when comparing the alpha–gamma coincidence measurements with the low-background singles gamma-ray spectrometry, the minimum detectable activities (MDA) are smaller in PANDA. For example, when studying ^{241}Am, the MDA achieved with PANDA was six times lower than with singles counting [Publication 2].

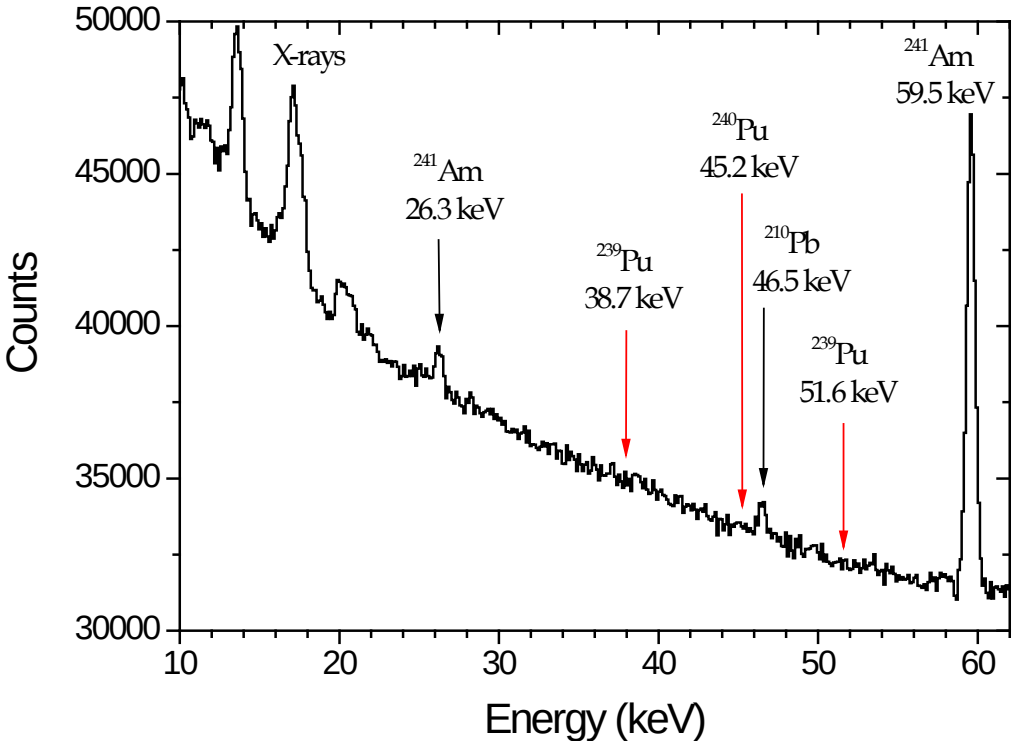

FIGURE 20. Singles gamma-ray spectrum of the Thule particle measurement in MP1. The positions of the Pu transitions of interest are marked in the spectrum with red arrows.

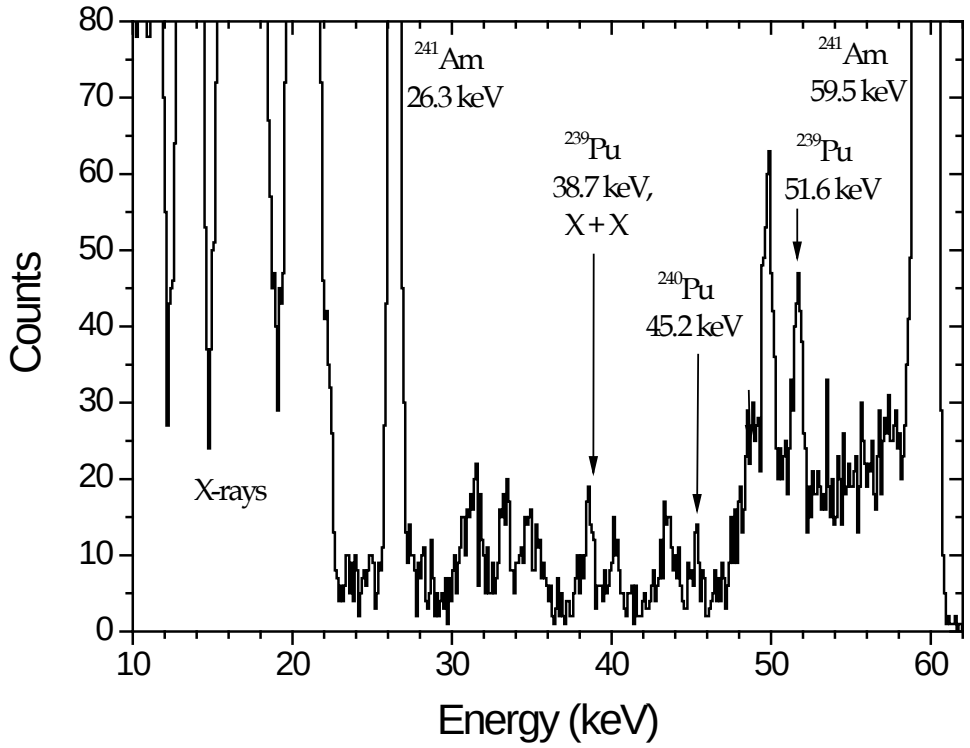

FIGURE 21. Alpha-gated gamma-ray spectrum of the Thule particle measurement in MP1. Besides the ^{241}Am peaks seen in the singles spectrum (Fig. 20), the ^{239}Pu and ^{240}Pu transitions of interest are now clearly visible. See Fig. 5 of [Publication 4] for an explanation of the rest of the spectrum.

A case with more than one radioactive particle in a sample was investigated in [Publication 2]. In this measurement, the sample contained five depleted uranium (DU) particles. The DU particles were larger than the Thule particle. Their diameters were approximately 100 µm each. Four of the particles were positioned in a row 1 cm from each other. The fifth particle was located right next to one of them (see Fig. 4 of [Publication 2]). The source-to-DSSSD distance in this measurement was 4.5 mm. The performed measurement showed that particles with 1 cm distance from each other can easily be separated and located rather accurately simply by viewing the hitmap of the DSSSD. As mentioned earlier, by using the particle-locating algorithm in SPANDA, particles much closer to each other can be separated.

By comparing the alpha spectrum of this and the Thule measurement, one may qualitatively examine the effect of particle size on the quality of the spectrum. For the larger DU particles, the shape of the alpha spectrum is almost flat due to the energy loss of the alpha particles in the sample material. It is also shown that the background in an alpha-gated gamma-ray spectrum is nearly zero. This allows the detection of ^{235}U transition at 185.7 keV (see Fig. 4 of [Publication 2]).

4.2.2 Swipes

Different kinds of swipes are commonly used to collect samples from surfaces. The International Atomic Energy Agency (IAEA) provided STUK reference and unknown swipe samples for the testing of the coincidence setup of MP1. These samples included two reference samples with known ^{240}Pu/^{239}Pu ratios and four unknown samples, of which only the amounts of Pu and U in the samples were provided. The sample properties provided by the IAEA (before any PANDA measurements were made) are presented in Table 2.

Table 2 IAEA swipe samples.

Sample ID	Swipe type	U contents	Pu contents	^{240}Pu/^{239}Pu
8146-01-27	Cotton	1 µg	1 ng	0.0298
8146-02-25	Cotton	1 µg	10 ng	0.132
8147-01-23	Cotton	1 µg	1 ng	-
8147-02-23	Cotton	1 µg	10 ng	-
30001-03-13	J-swipe	-	1 pg	-
30001-04-13	J-swipe	-	1 pg	-

The reference samples were cotton swipes with an area of approximately 105 mm * 105 mm. One of these was measured in MP1. Two of the unknown samples were cotton swipes and two were J-swipes (absorbent cellulose). The

diameter of each of these four unknown swipe samples was approximately 25 mm. Three of the unknown samples were measured in MP1. Photos of a reference and an unknown sample are presented in Figure 22.

FIGURE 22. IAEA swipe samples. The two reference samples were large square-shaped swipes like sample 8146-01-27 on the left and the four unknown samples smaller round swipes like sample 8147-01-23 on the right.

The measurement and analysis of reference swipe 8146-02-25 was presented in [Publication 3]. This sample was measured twice in MP1. The first 30.7 d measurement demonstrated that the sample contained a large amount of ^{241}Am, which interferes with the Pu analysis. Figure 23 presents the alpha-gated gamma-ray spectrum from the energy range 3 to 64 keV. This spectrum clearly shows the massive ^{241}Am contribution. The presence of ^{241}Am makes the ^{239}Pu and ^{240}Pu analysis difficult, since it causes extra sum peaks in the region where the Pu peaks are located. These sum peaks are not at the exact same energies as the main Pu peaks (^{239}Pu, 51.6 keV and ^{240}Pu, 45.2 keV).

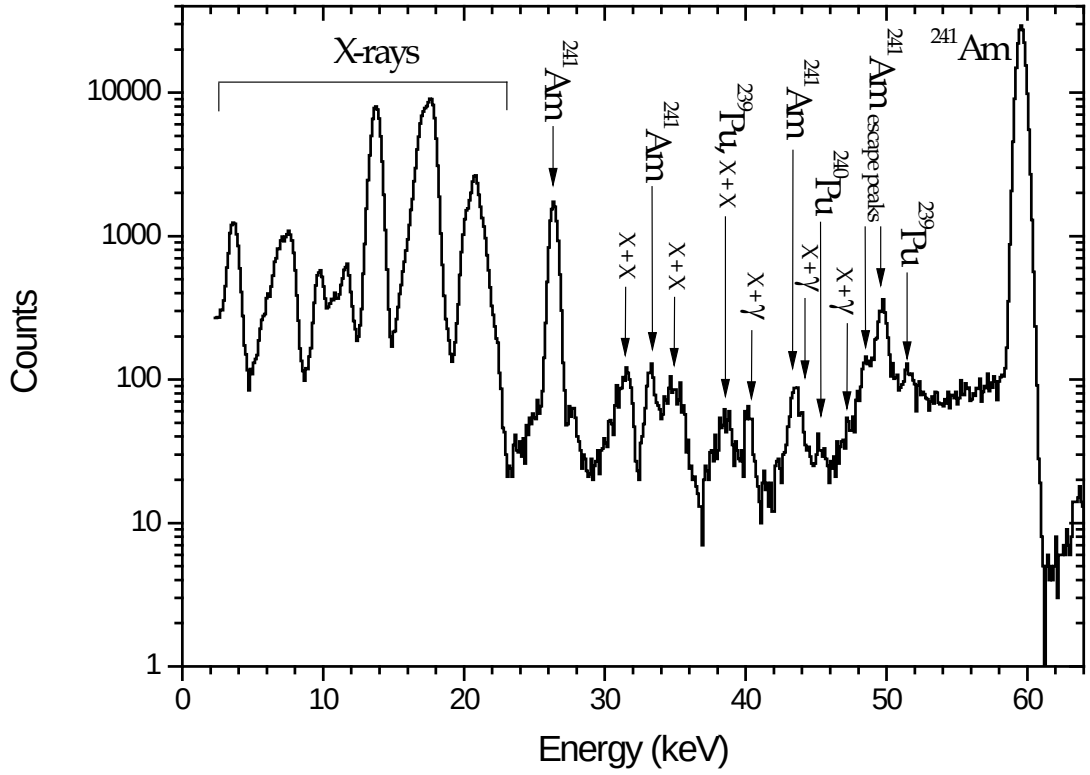

FIGURE 23. Alpha-gated gamma-ray spectrum of IAEA swipe sample 8146-02-25.

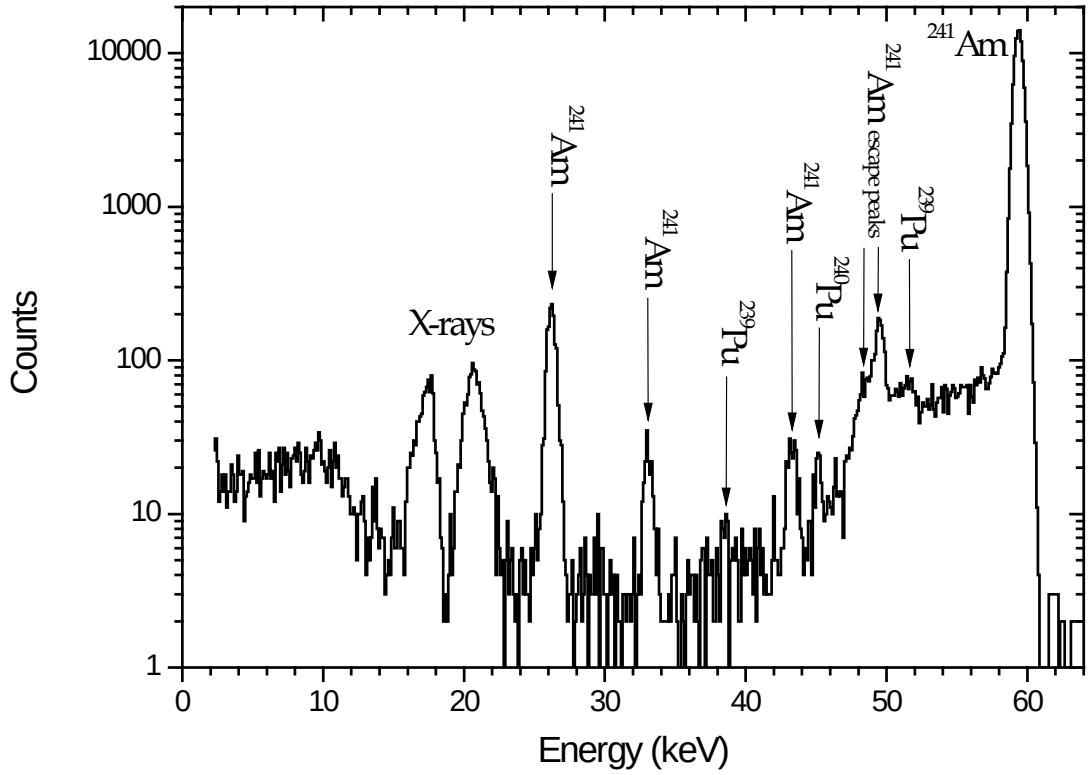

FIGURE 24. Alpha-gated gamma-ray spectrum of IAEA swipe sample 8146-02-25 using an absorber foil. A 300 μm Ti foil was used as an attenuator between the sample and the BEGe detector.

In the second 16.7 d measurement, a 300 µm thick Ti foil was installed between the BEGe detector and the sample. This was in order to absorb the low-energy X-rays that cause the Am sum peaks near the Pu peaks. The total alpha-gated gamma-ray spectrum using the Ti foil attenuator is presented in Figure 24. As shown, the Ti attenuator completely removes the sum peaks from the spectrum. Obviously, the peaks of interest are also a little smaller when the Ti foil was used. The main benefit of the attenuator is seen with the ^{240}Pu peak located at 45.2 keV. This peak is much better defined in the measurement where the Ti foil was used than in the case where it was not used. A slightly thinner Ti attenuator would have probably produced even better final results, i.e., the statistics of the peaks of interest would have been larger and the background would still have been low. Figure 4 of [Publication 3] is a blow-up of the region where the Pu peaks are located. It also shows the results of the peak analysis.

Figure 3 of [Publication 3] shows that it is possible to examine the alpha particle distribution of a single nuclide present in a swipe sample. The two-part figure contains the whole alpha particle hitmap created using the DSSSD data and an ^{241}Am (59.5 keV) gamma-gated alpha particle hitmap. The ^{241}Am distribution closely follows the overall distribution of alpha particles emitted by the sample. While investigating the homogeneity of the samples, studies of this kind are useful.

Figure 5 of [Publication 3] presents the singles alpha spectrum and a 59.5 keV gamma-gated alpha spectrum of the DSSSD from a two day period. The shape of the gated alpha spectrum is useful when analysing the total alpha spectrum. The shapes of the alpha spectra also reveal that part of the radioactive material is located deep inside the swipe material.

The three unknown swipe samples that were studied also proved to be challenging. The hitmaps created from the DSSSD data of each sample showed that two of the unknown samples had the radioactive material spread over a large area, as in the reference sample. The alpha particle hitmap of the least active unknown sample (1 pg of Pu) had a single spot, hinting that it could either contain a single particle or that the radioactive material was simply spread out on a very small area. The presence of Pu could not be confirmed from this sample. The detection was based on ^{241}Am (see also Table 3).

The studied swipe samples were produced in a way that the majority of the alpha particles were not able to escape the sample matrix. Approximately only one-eighth of the alpha particles emitted towards the DSSSD could be detected [Publication 3]. Therefore, better quality samples would have saved measurement time. The results obtained from the analysis of the swipe samples are presented in Table 3. ^{240}Pu/^{239}Pu enrichment information provided afterwards by the IAEA is also added to this table.

Table 3 Results from the analysis of IAEA swipe samples.

Sample ID	$^{240}Pu/^{239}Pu$ from IAEA	$^{240}Pu/^{239}Pu$ measured	Pu-239 activity [Bq]	Pu-240 activity [Bq]	Am-241 activity [Bq]
8146-02-25	0.132	0.12 ± 0.03	30 ± 8	15 ± 3	16 ± 1
8147-01-23	0.030	0.06 ± 0.05	3.5 ± 0.8	0.8 ± 0.5	0.053 ± 0.007
8147-02-23	0.132	0.15 ± 0.06	25 ± 4	14 ± 4	15.3 ± 0.3
30001-03-13	Pu not detected				0.001 - 0.06

When qualitatively comparing the IAEA reference swipe 8146-02-25 and the Thule particle presented in the previous section, some observations can be made. In the Thule particle the enrichment of ^{239}Pu was determined to be ~95%, whereas in the swipe the enrichment was ~88-89%. This difference can also be seen when comparing the sizes of the peaks located at energies 45.2 keV (^{240}Pu) and 51.6 keV (^{239}Pu) in both cases. In the swipe sample spectrum presented in Figure 24, the peaks are rather equal in size, whereas in the Thule particle spectrum presented in Figure 21 the 51.6 keV is several times larger than the 45.2 keV peak.

The relative amount of ^{241}Am as compared to ^{239}Pu was approximately four times greater in the swipe sample than in the Thule particle. As mentioned earlier, the presence of large amounts of ^{241}Am makes the determination of the Pu peaks much more challenging, since it masks the main transitions of ^{239}Pu and ^{240}Pu in the alpha-gated gamma-ray spectra (see Figs 23 and 24).

The sample type has a significant effect on the quality of the data. This and also the influence of the large amount of ^{241}Am can be seen when comparing the results obtained for the $^{240}Pu/^{239}Pu$ atom ratios in both cases: Thule particle $^{240}Pu/^{239}Pu = 0.053 \pm 0.011$, swipe sample $^{240}Pu/^{239}Pu = 0.12 \pm 0.03$. The data acquisition times were 21 days and 17 days, respectively. The atom ratio could be determined more precisely for the Thule particle, even though it only contained about one-tenth of the Pu in the swipe sample:

Thule	(1.5 ± 0.2) ng of ^{239}Pu
	(0.08 ± 0.02) ng of ^{240}Pu
Swipe:	(13 ± 3) ng of ^{239}Pu
	(1.8 ± 0.4) ng of ^{240}Pu.

4.2.3 Air filters

Radioactive substances in outdoor and indoor air are monitored by collecting air samples on various types of filters for later spectrometric analysis. An MP1 measurement of an air sample was presented in [Publication 2]. The sample was collected in STUK's underground garage using a Lilliput air sampler. Figure 25 presents the fluoropore filter that was used in sample collection.

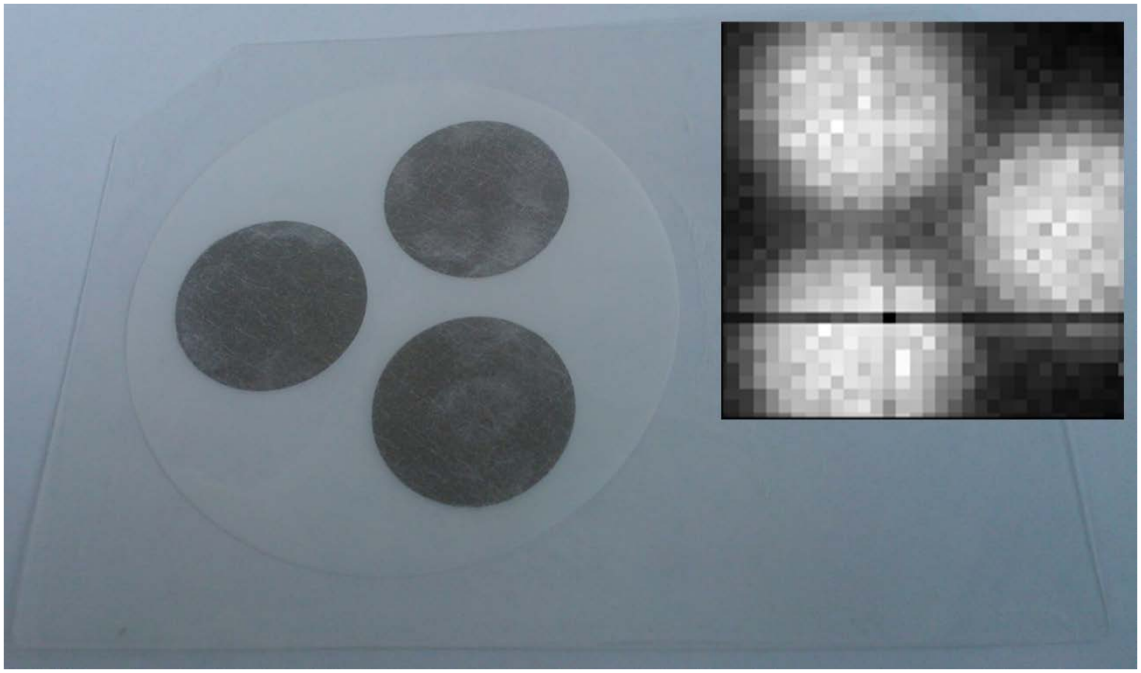

FIGURE 25. Laminated fluoropore air filter. The three grey areas (diameter 32 mm each) are the inlets of the air flow. The top right insert shows the alpha particle hitmap created from the DSSSD data (figure taken from [Publication 2]). The lighter the colour, the more alpha particles have been registered.

The sample collection time was 2.2 h and the MP1 measurement lasted 3 d 5 h. The delay between the end of the sample collection and the start of the data acquisition was 30 min. The insert in Figure 25 shows that the radon progenies collected on the filter are distributed evenly, i.e. the shape of the alpha particle hitmap created from the DSSSD data closely follows the shape of the three-part air filter. The resulting alpha spectra are also of relatively good quality (see insert in Fig. 26). Therefore, quite pure alpha-gated gamma-ray spectra can be created from the measurement data (see Fig. 5c of [Publication 2]).

Since in the data acquisition of MP1 each single event is time stamped, it is possible to study the time behaviour and half-lives of the nuclides present in the samples. This is illustrated in Figure 26, in which the time behaviour of three alpha-decaying radon progenies (^{212}Bi, ^{212}Po and ^{214}Po) present in the sample is shown. Tailing of the alpha peaks causes some disturbance in the time behaviour plots of ^{212}Bi and ^{214}Po. For half-life and decay chain information on the nuclides, see Appendix 2.

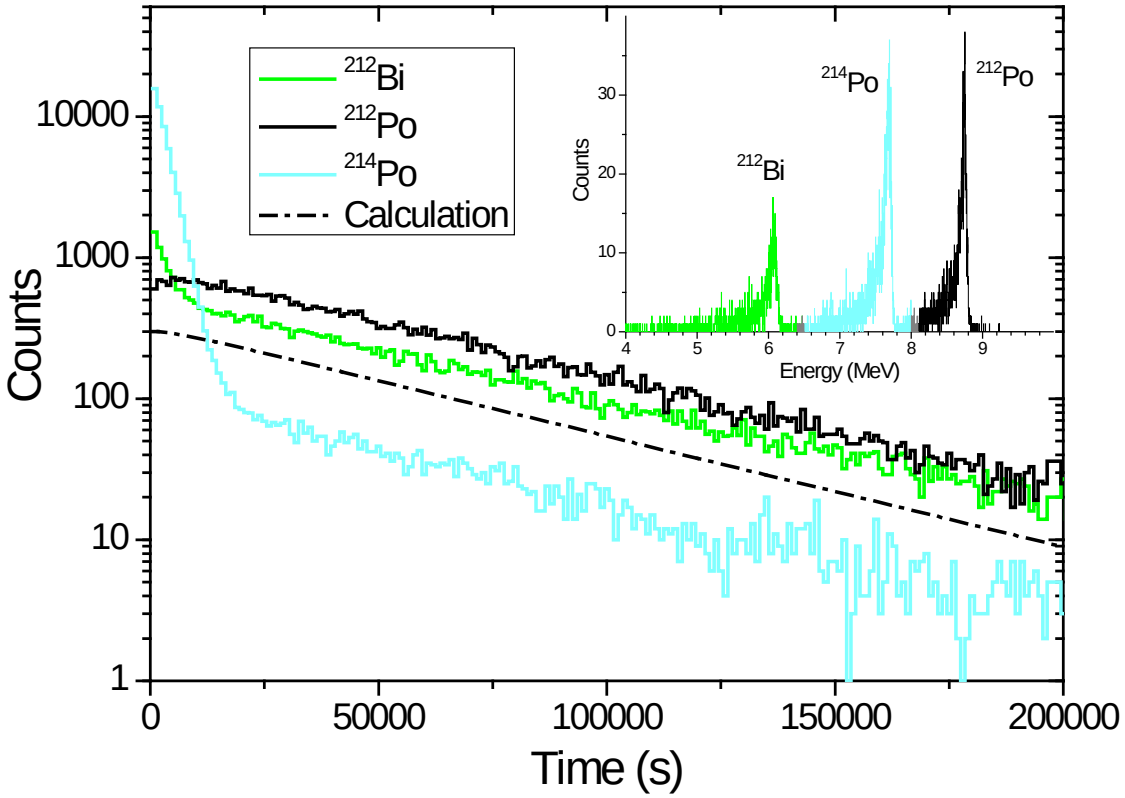

FIGURE 26. Time behaviour of ^{212}Bi, ^{212}Po and ^{214}Po. The energy regions (alpha peaks) used in the creation of the time behaviour curves are shown in the insert. The figures are taken and modified from [Publication 2].

PANDA has also been tested and used with air samples containing radioactive material not occurring naturally in the environment. One example presented here is a case where radioactive materials were accidentally released in a steel factory that recycles scrap metal as a raw material [27]. Air samples collected at the site showed clear traces of ^{241}Am, even in singles gamma-ray spectrometry. Some of these air filters were further analysed using PANDA. The case presented here is a sample that contained 3 Bq of ^{241}Am. The filter is shown in Figure 27. As seen from the picture, the filter is dirty. Therefore, it can be assumed that part of the alpha particles deposit all of their energy in the sample matrix and never enter the DSSSD. The overall diameter of the filter was 100 mm and the diameter where the sample was collected was 92 mm.

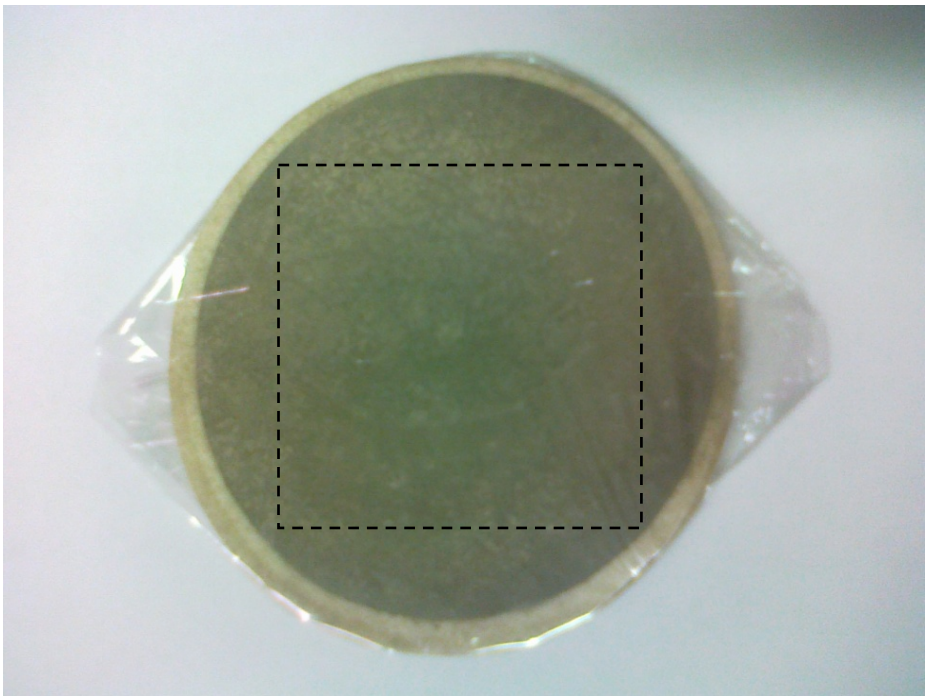

FIGURE 27. Air sample collected on a filter at a steel factory. The filter is covered with a 2.5 µm thick Mylar foil. The dashed line shows the area of the DSSSD detector.

The PANDA measurement lasted a total of 5 d 17 h. The alpha particle hitmap created using the DSSSD data is presented in Figure 28. The hitmap shows that the radioactive substances are spread out rather equally through out the entire filter and no single particle with a much higher than average activity is present. Note that since the diameter where the sample is collected is 92 mm and the size of the DSSSD is smaller than this (64 x 64 mm^2), the edges of the filter are not visible to the DSSSD. The same filter was also imaged using an autoradiography technique. The exposure time was 6.9 d. The results of the autoradiography were in line with the ones obtained from the DSSSD hitmap and showed no single particles with anomalous activity.

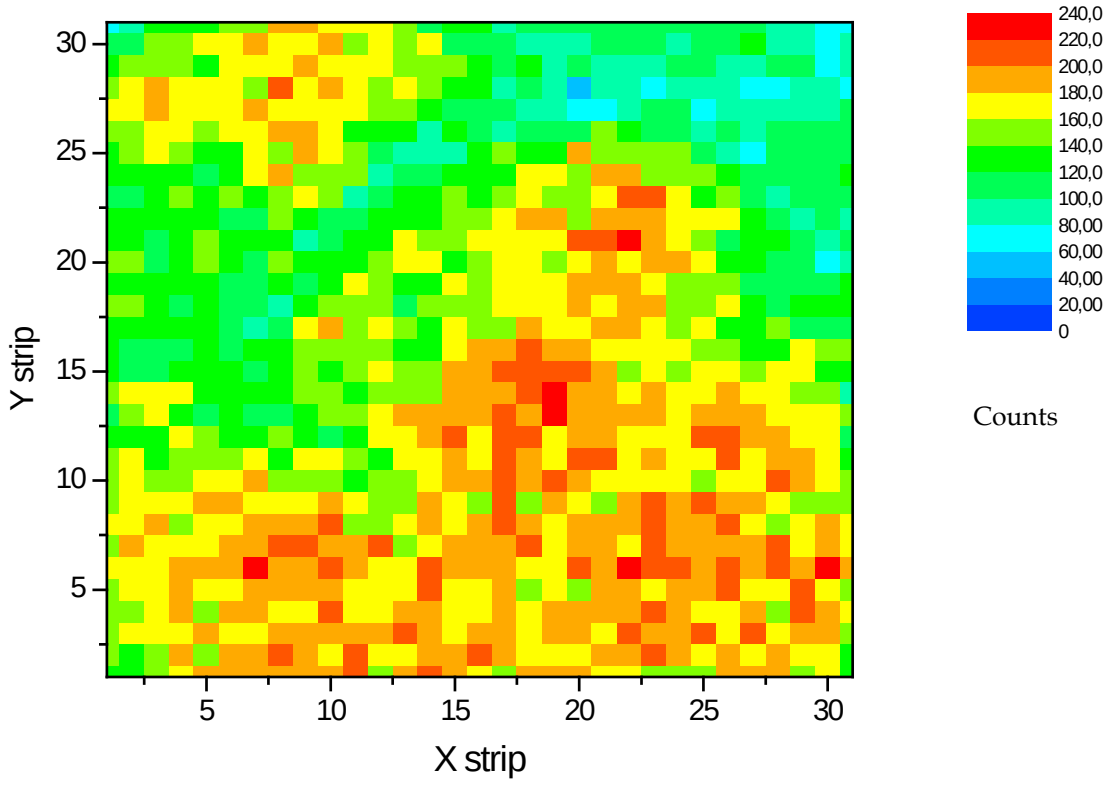

FIGURE 28. Alpha particle hitmap of an air sample containing ^{241}Am.

The alpha-gated gamma-ray spectrum is presented in Figure 29. No other nuclides than ^{241}Am could be found. The small peaks not marked on the spectrum are caused by the earlier-discussed summing of multiple ^{241}Am gamma and X-rays. Data analysis gave an activity estimation of 2 Bq. Note that the measurement geometry is not optimal for such a large sample, since the DSSSD is able to directly see only about two-thirds of the filter surface. This also explains the difference in the activity estimation if compared to the result of singles gamma-ray spectrometry.

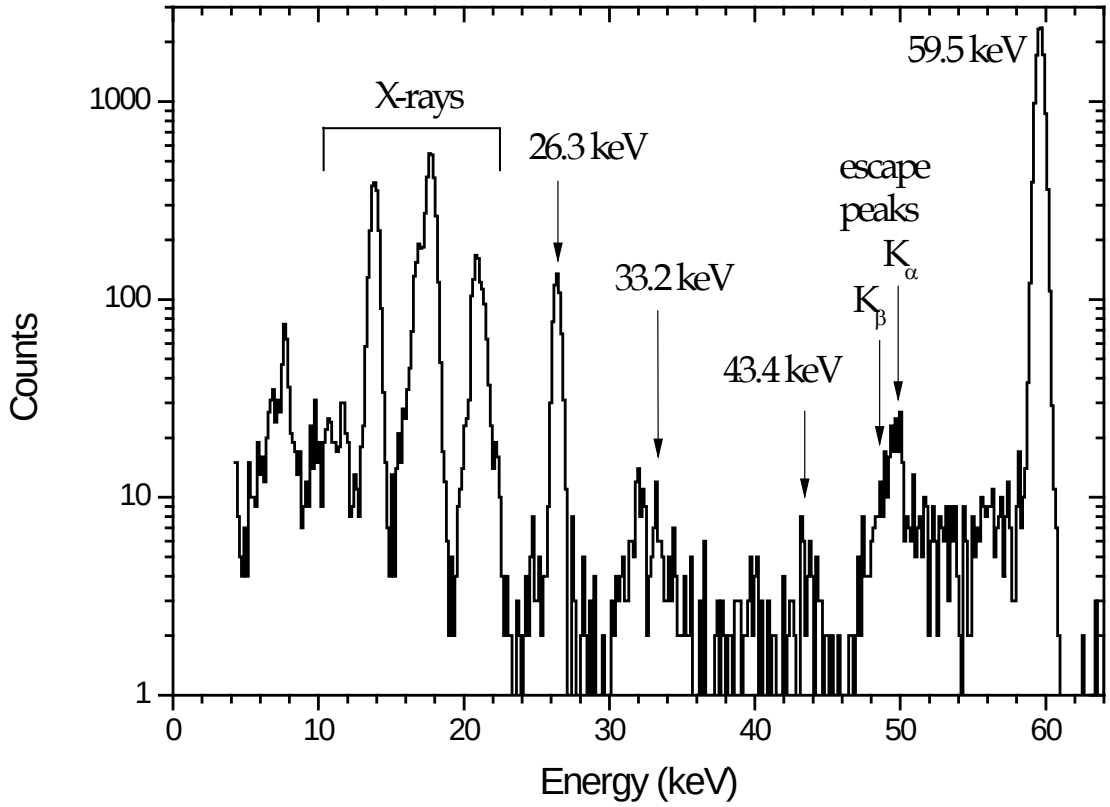

FIGURE 29. Alpha-gated gamma-ray spectrum of an air sample containing ^{241}Am.

4.2.4 Impactor samples

Impactor samples for the studies were provided by Erich Hrnecek of the Joint Research Centre – Institute for Transuranium Elements (JRC-ITU) in Karlsruhe, Germany. These samples were prepared by collecting aerosols that originate from tungsten inert gas welding. This was done with a Berner low-pressure impactor. PANDA measurements were carried out for two impactor samples, which are referred to as T1_016 and T1_017. Both samples were measured on two different occasions. In the first measurements, only the DSSSD was used. The second measurement also involved the BEGe detector and the alpha–gamma coincidence system of MP1. Photos of these two impactor samples are presented in Figure 30.

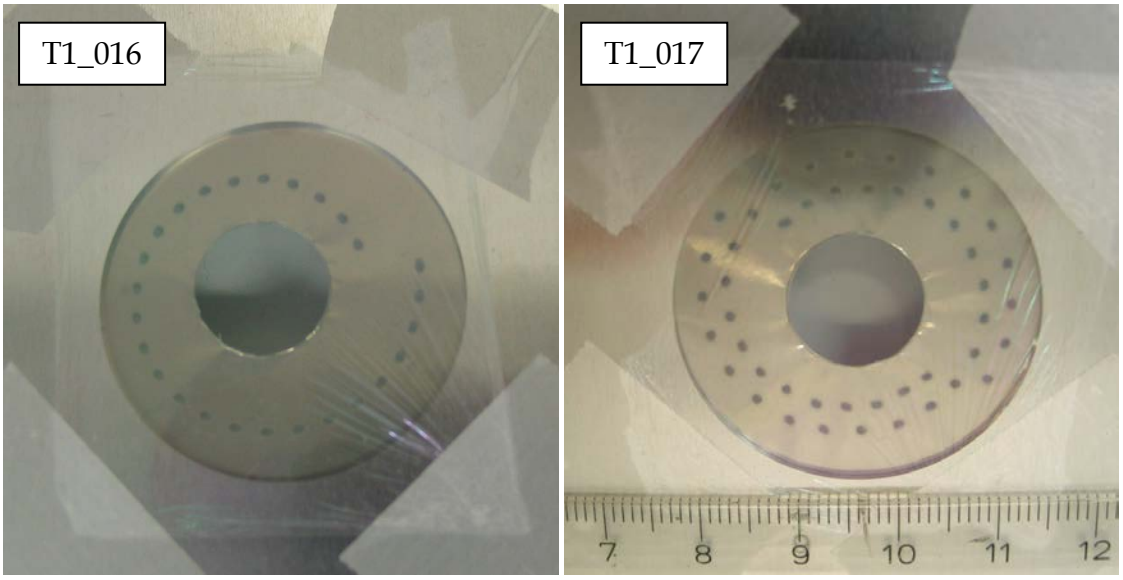

FIGURE 30. Impactor samples T1_016 and T1_017. The protecting Mylar foils are attached to the sample holder plates on top of the samples to prevent the foils from touching the surfaces of the samples.

Both impactor samples measured with PANDA had a spiral shape. Sample T1_016 had a single loop while sample T1_017 had two loops. The loops were composed of spots with a size of approximately 1 mm and a distance of 3–4 mm between consecutive spots.

In the first measurement of sample T1_016, the sdd was 4 mm and the Mylar foil protecting the sample was 1 mm from the sample surface (see Fig. 30). This measurement was used in the study of electrostatically charged foils [Publication 5], which is presented in the next section. Later, the same sample was measured with an sdd of 3 mm which can be considered the minimum easily achievable sdd with the DSSSD. This time the Mylar foil was installed directly on the surface of the sample. One goal with these measurements was to test the effect of the sdd on the quality of the hitmap images created with the DSSSD.

Alpha particle hitmaps using sdds of 3 and 4 mm are presented in Figure 31. This figure also presents an image of the sample obtained using the autoradiography technique. The hitmaps reveal that a 1 mm difference in the sdd can have a significant effect on the quality of the created hitmap image. Since the pixel size of the DSSSD is 2 mm * 2 mm and the minimum sdd is around 3 mm, it is clear that single spots cannot be distinguished from each other.

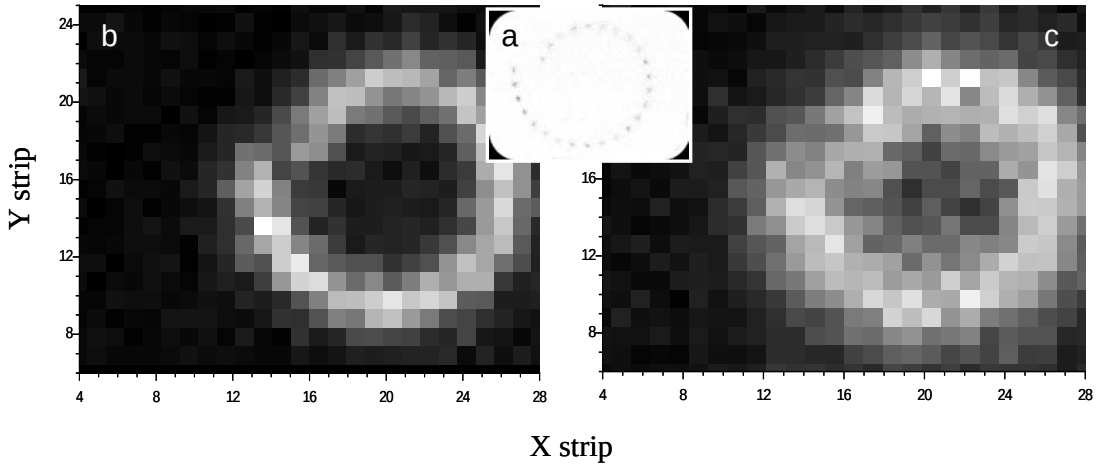

FIGURE 31. Alpha particle hitmaps of impactor sample T1_016. (a) Autoradiography image of the sample. (b) Alpha particle hitmap created from DSSSD data when sdd is 3 mm. (c) Alpha particle hitmap created from DSSSD data when sdd is 4 mm. Figure taken from [28].

The first measurement of sample T1_017 was also made to test the DSSSD image quality. The second measurement of this sample was carried out in order to prove that the electrostatic collection of radon progenies on the protecting Mylar foils seen in the measurement of sample T1_016 could be reproduced (see next section).

4.2.5 Electrostatically charged foils

The samples measured in PANDA are typically covered with Mylar foils in order to protect the detectors from contamination. These foils can sometimes be electrostatically charged [29] and [30]. Charged foils are able to collect aerosols from indoor air. If the concentration of radon progenies in the air is high, this may lead to unwanted contamination of the foil surface. This can cause serious problems when analysing the measurement data.

One of the impactor samples discussed earlier, T1_016, was covered with a 0.5 µm Mylar foil and then left overnight in the laboratory where the PANDA device is located. The measurement was started the following day. The results proved to be interesting and led to further studies of electrostatically charged foils, Mylar in particular. The collection and behaviour of radon progenies on Mylar foils was reported in [Publication 5].

At the beginning of the measurement of sample T1_016, the alpha particle hitmap did not look as would have been expected. The time behaviour of the sample during the first part of the measurement (RUN153, 17.3 h) was studied in detail. The data was binned to 200 s bits. After this, the run was divided into two parts. The first part was the beginning of the run (gate 1: from 0 to 3 h) and the second part was the rest of it (gate 2: from 3 to 17.3 h). Figure 32 presents the alpha-gated timestamp data.

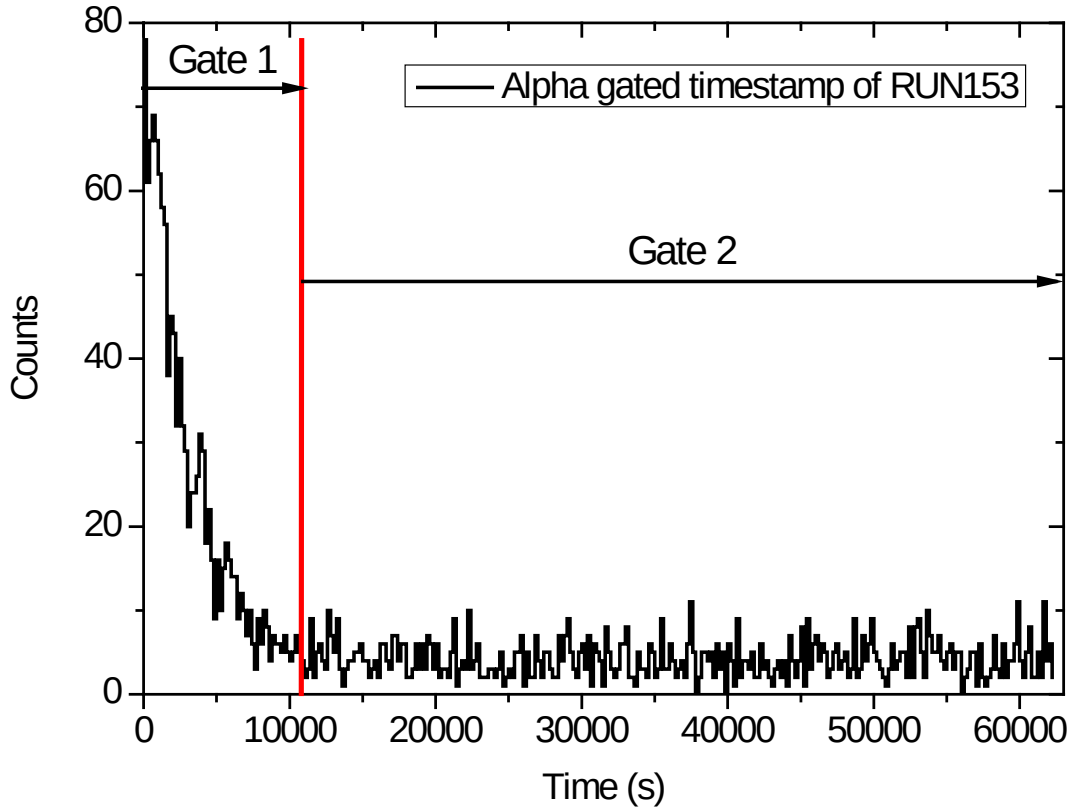

FIGURE 32. Alpha-gated time behaviour of impactor sample T1_016. The alpha gate was approximately from 1.9 to 9.8 MeV.

The alpha particle hitmaps created using the first three hours of the measurement and the rest of the data are presented in Figure 1 of [Publication 5]. The alpha particle hitmap from the start of the measurement (3 h) is different from the hitmap of the longer period (13.9 d). The alpha spectra of these two periods are also shown in the same figure. The whole 14 d measurement is presented here in Figure 33. The marked peak at 7.7 MeV belongs to ^{214}Po and it is not from the actual sample but from aerosols collected on the surface of the Mylar foil. ^{214}Po is a naturally occurring radon progeny originating from the uranium series (see Appendix 2). When analysing a spectrum like the one in Figure 33, it would be very hard to tell that this peak does not originate from the actual sample, leading to false results.

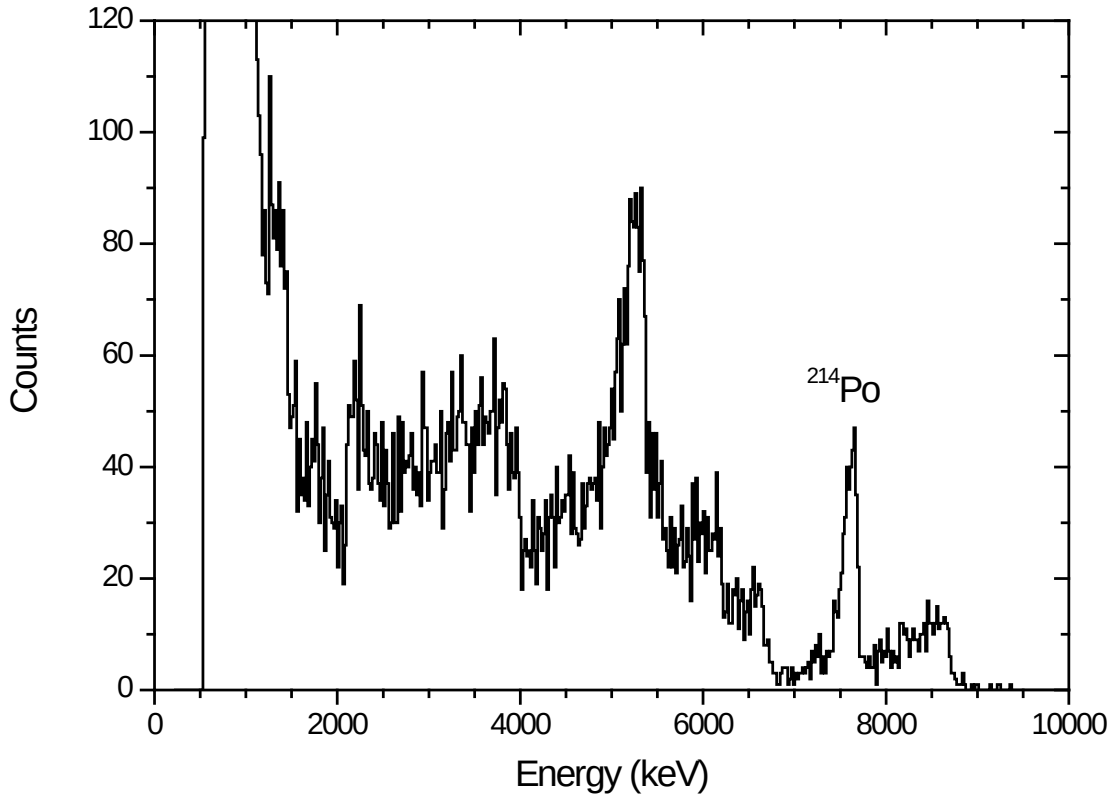

FIGURE 33. Total alpha spectrum of the 14 d measurement of impactor sample T1_016. Alpha spectra from partial measurement periods are presented in Fig. 1 of [Publication 5].

Properties of plain Mylar foil without an actual sample were also investigated. STUK's garage was chosen as the sample collection site, since it was known that the concentration of radon progenies is rather high (usually > 100 Bq/m^3). In the garage, plain Mylar foil was spread out on one of PANDA's sample holder plates, which had a hole of 35 mm diameter. The Mylar in this area was not in contact with anything other than the air of the garage. After two hours, the sample holder was retrieved from the garage and measured in PANDA. The delay between the end of the sample collection and the start of the measurement was 30 min. An 18 h measurement in PANDA demonstrated that radon progenies were collected on the foil. Figure 34 shows the time behaviour of nuclides ^{212}Bi, ^{214}Po and ^{212}Po. The same figure was presented in [Publication 5] without ^{212}Bi. The time behaviour of each of these nuclides verifies that the radon progenies do not escape from the Mylar foil, even in vacuum conditions. Their amount decreases only through radioactive decay, closely following the theoretical prediction. In comparison to Figure 26, note now the effect of the better spectrum quality, i.e., less tailing of the alpha peaks.

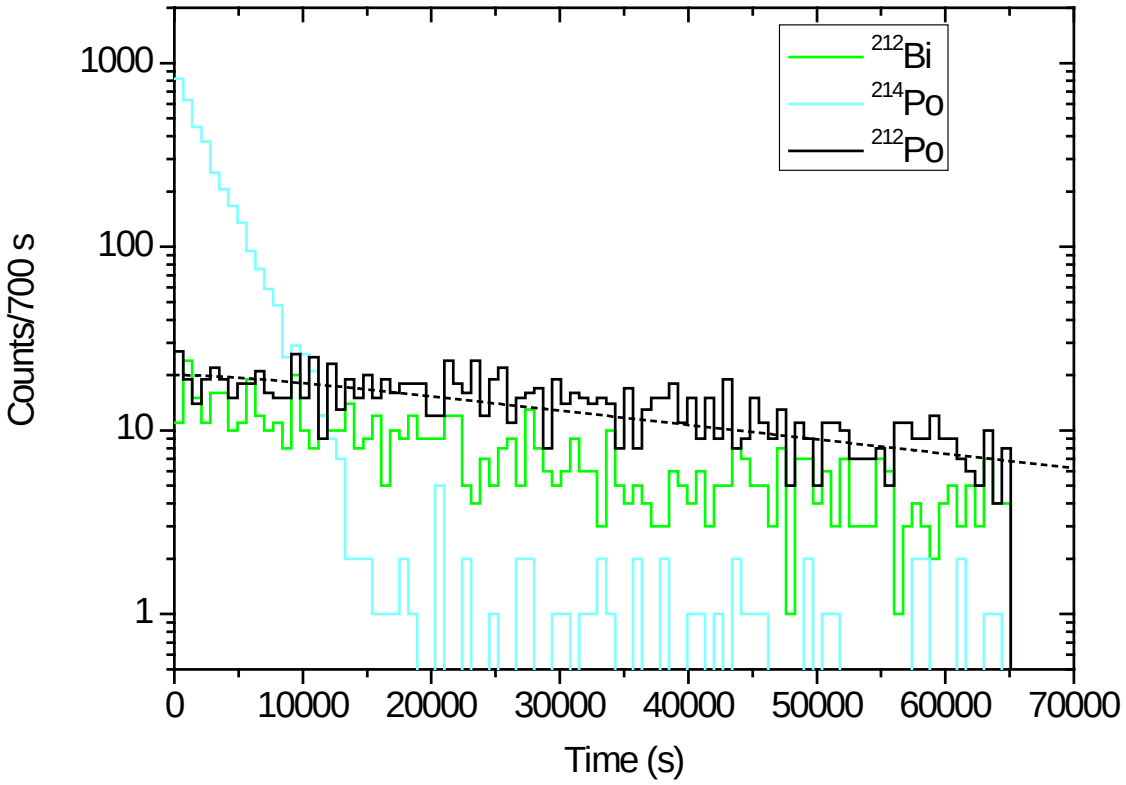

FIGURE 34. Time behaviour of ^{212}Bi, ^{214}Po and ^{212}Po on the Mylar foil. The figure is modified from Fig. 2 of [Publication 5]. ^{212}Bi was omitted from the original figure to simplify the picture.

In addition to the PANDA measurements, Mylar foils were also measured *in situ* in STUK's garage with a CAM PIPS detector (Canberra model CAM450AM). The CAM PIPS is a detector designed for continuous air monitoring and it can be used in ambient air pressure. In these measurements, the radon concentration in the air was monitored with a portable AlphaGUARD radon monitoring device. As can be seen from Figure 3 of [Publication 5], the Mylar foil is able to collect radon progenies quite efficiently for approximately 3 hours. After this time period, the activity of the sample starts to decrease, since the foil is discharged and no new aerosol particles containing radon progenies are collected on the foil surface. The collection rate of radon progenies on a small piece of Mylar foil was found to be equivalent of an air sampler with a flow rate of 0.1 m^3/h. This can be considered rather efficient, since the method does not require any power source to operate.

4.3 Analysis of samples with MP2

PANDA's Measurement Position 2 (MP2) was reported in [Publication 6]. To assess the performance of the SDD detector, two measurements of an ^{241}Am sample were made. This source was prepared by dropping liquid containing ^{241}Am on a piece of 6 µm thick Mylar foil. After this the liquid was vaporized and the residue spot, with a diameter of 1–2 mm, was covered with 0.5 µm thick Mylar foil. The activity of the sample was approximately 28 Bq.

The first measurement was carried out with the sample as such. For the second measurement, additional Mylar foil with a thickness of 48 µm was installed on top of the 0.5 µm thick foil. The data acquisition time in the first measurement was 24 h and in the second 22 h. The SDD in both measurements was approximately 10 mm. The spectra obtained in these measurements are presented in Figure 35.

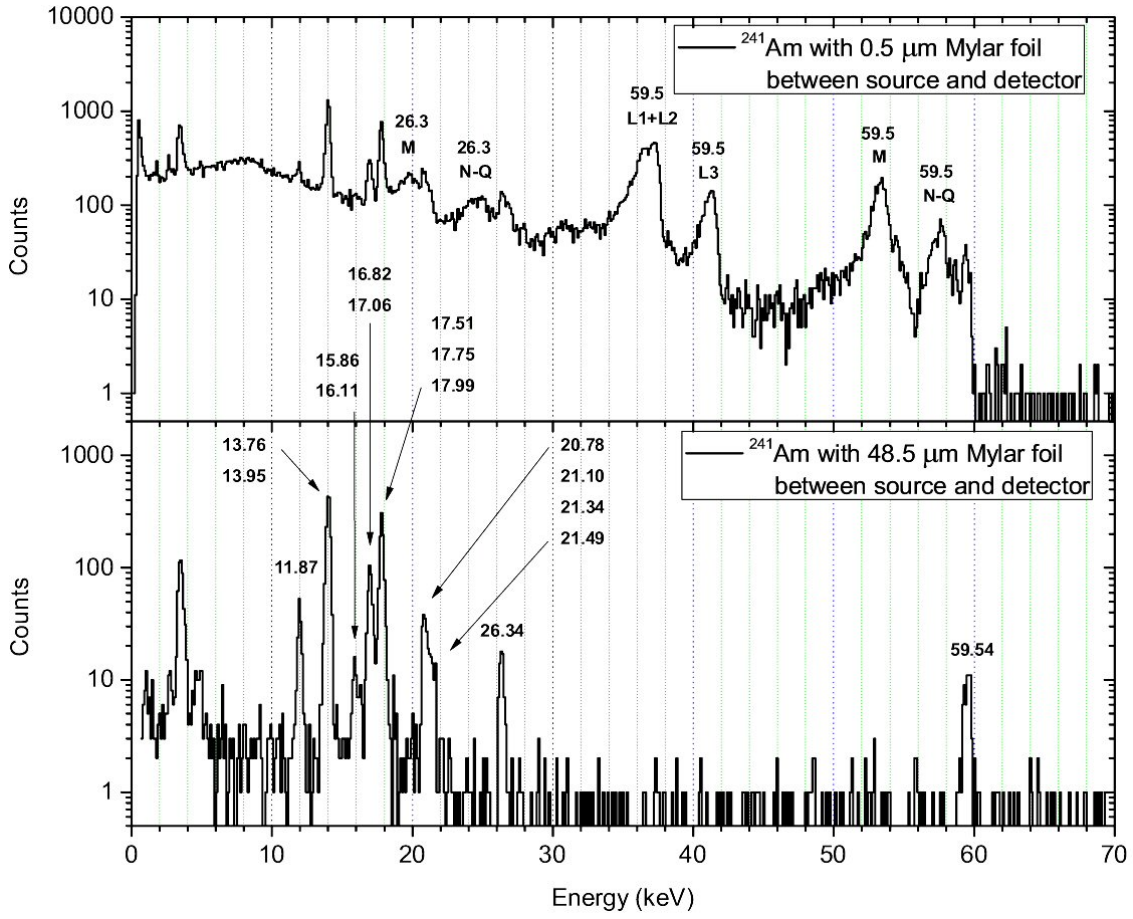

FIGURE 35. Conversion electron/photon spectra recorded with the SDD. In the measurement of the upper spectrum, the sample was covered with a 0.5 µm thick Mylar foil. For the lower spectrum, additional Mylar foil with a thickness of 48 µm was used. The figure is taken from [Publication 6].

The first measurement demonstrated that MP2 can be used to simultaneously measure conversion electrons and X-rays. When studying the conversion electron peaks, one can see that the L1 (35.7 keV) and L2 (36.6 keV) transitions related to the 59.5 keV gamma ray form a duplet with a visible minimum. This means that conversion electron peaks located closer than 1 keV to each other could be separated and analysed if appropriate analysis software were available. Note that measurements without the protective Mylar foil between the sample and the detector could also be planned. This would further improve the energy resolution.

If only the X-rays (and possible low-energy gamma rays) are of interest, the electrons can be removed from the spectrum using an attenuator of appropriate thickness. A relatively thin layer of material (48.5 µm of Mylar) is able to stop electrons of these energies. Such material thicknesses have a minor effect on the transmission of the X-rays. The X-ray spectra can reveal properties of elements present in the sample. The SDD in MP2 has a far better resolution than the BEGe in MP1. Experimentally determined resolutions (FWHM) at 17.7 keV were 1.7% for the SDD and 3.4% for the BEGe. Using MP2 makes the analysis of the X-ray multiplets easier.

The use of MP2 with unknown samples still requires a considerable amount of work. No current operational analysis software is capable of analysis of conversion electron spectra. The main difference is the peak shape produced by conversion electrons compared to those of photons. Also, we do not have a program dedicated to the analysis of beta spectra (^{241}Pu). However, specific analysis software for electron spectrometry is under development. Another challenge is the conversion electron yields of many actinides, since these are not known very precisely. For the absolute analysis of samples, the conversion electron yields have to be known accurately. If better data are not produced elsewhere, these could in principle be determined using MP2.

5 DISCUSSION AND OUTLOOK

The traditional measurements and analysis of samples rely on techniques such as a single detector and a multichannel analyser. The NDA project and the PANDA device have provided new perspectives and improved STUK's sample analysis capability and the entire measurement process.

The positive results obtained with coincidence techniques and recording the data in list mode have been taken into use in many other devices. For example, the so-called MiniPANDA device is an alpha–gamma coincidence measurement setup that is basically a simplification of PANDA's MP1. MiniPANDA has a BEGe detector (similar as in PANDA) and a planar CAM PIPS detector from Canberra. The detectors face each other inside a lead castle. The samples are studied between the detectors in normal air pressure. Previously, the data collection was performed using hardware coincidence instead of software coincidence, but the data acquisition system was updated to a digital one in 2012.

A simplified alpha–gamma coincidence system was also designed and constructed for the steel factory mentioned in section 4.2.3. This is a user-friendly device for on-site nuclide identification from air samples and it has been successfully operated in an industrial environment since spring 2012. Another application of the coincidence technique was to replace a conventional alpha detector with a UV detector. As the NDA project progressed, the UV research diverged to form a project of its own. Development along these lines will also continue in the future.

The use of time-stamped list mode data acquisition is the key to success in the future. This data acquisition method has been or is planned to be implemented in several existing and future measurement devices of STUK. For example, neutron spectrometry using borated plastic scintillators is impossible without the list mode data storage format. Other in-field techniques also greatly benefit from this data-acquisition method (source localization, noise reduction, etc.). Globally, it seems that there is an ongoing transition from traditional data acquisition to list mode data acquisition. The development of sophisticated

multidetector setups and novel detectors is accelerating this transition. In this context, PANDA has been a pioneer.

The four-year NDA project ended in 2011. The work is continuing in the SPED project of STUK. Many techniques developed and tested during the NDA project will be applied in new instruments that are to be used in the laboratory and also in the field measurements.

During the SPED project, the development of the PANDA device will continue. Future plans for PANDA include replacing the SDD of MP2 with a similar but larger area detector and also splitting the energy signal of the SDD to simultaneously produce both the X-ray/electron spectrum (~ 0−100 keV) and the alpha spectrum (~ 0.5−10 MeV). Some research is also planned in order to further reduce the intensity of the ^{241}Am sum peaks in the alpha–gamma coincidence spectra without losing the X-ray information.

Finally, a thick (1500 µm) Si detector with a surface area equal to the DSSSD (64 x 64 mm^2) will be installed behind the DSSSD and tested for the detection of beta particles. If successful, it may also be possible to study the distribution of beta emitters in samples (BEGe, Si, DSSSD coincidence). This feature would be useful in the aftermath of nuclear incidents when trying to locate and identify fission products in samples. The PANDA device was used after the Fukushima Daiichi nuclear accident, which was caused by an earthquake and tsunami in Japan on 11.3.2011. Air filters collected from Tokyo and swipes taken from the surfaces of planes flying from Helsinki to Tokyo, Osaka and Seoul and back were measured with PANDA. The measurements confirmed that alpha-decaying nuclides were not present in these samples.

REFERENCES

[1] Safeguards Techniques and Equipment. –Rev. ed.- 2003. Vienna: International Atomic Energy Agency, ISBN 92-0-109403-5.

[2] Westlén, D. 2007. Reducing radiotoxicity in the long run. Progress in Nuclear Energy 49 (8), 597-605.

[3] Christodouleas, J.P., Forrest, R.D., Ainsley, C.G., Tochner, Z., Hahn, S.M., Glatstein, E. 2011. Short-Term and Long-Term Health Risks of Nuclear-Power-Plant Accidents. New England Journal of Medicine 364, 2334-2341.

[4] Cochran, T.B. and Paine, C.E. 1995. The Amount of Plutonium nad Highly-Enriched Uranium Needed for Pure Fission Nuclear Weapons. Nuclear Weapons Databook. Natural Resources Defence Council, Inc. Washington D.C. Revised 13.4.1995.

[5] Ring, J.P. 2004. Radiation risks and dirty bombs. Health Physics 86, 42-47.

[6] Karam, P.A., 2005. Radiological Terrorism. Human and Ecological Risk Assessment: An International Journal 11 (3), 501-523.

[7] Harrison, J., Leggett, R., Lloyd D., Phipps A., Scott B. 2007. Polonium-210 as a poison. Journal of Radiological Protection 27, 17-40.

[8] McFee, R.B., Leikin, J.B. 2009. Death by Polonium-210: lessons learned from the murder of former Soviet spy Alexander Litvinenko. Seminars in Diagnostic Pathology 26 (1), 61-67.

[9] Krane, K.S. 1988. Introductory nuclear physics. John Wiley & Sons, New York, ISBN 0-471-85914-1.

[10] Lilley, J. 2001. Nuclear physics – Principles and applications. John Wiley & Sons Ltd, Chichester, England, ISBN 0-471-97936-8.

[11] http://www.nndc.bnl.gov/ensdf/ (accessed 26.3.2013)

[12] Cottingham, W.N. and Greenwood, D.A. 2001. An introduction to nuclear physics, Second edition. Cambridge University Press, United Kingdom. ISBN 0-521-65733-4.

[13] http://www.nucleide.org/DDEP_WG/DDEPdata.htm (accessed 26.3.2013)

[14] Lhersonneau, G. 1993. Nuclear Spectroscopy. The 3rd international summer school. University of Jyväskylä, Department of Physics.

[15] Moring, M., Ikäheimonen, T.K., Pöllänen, R., Ilus, E., Klemola, S., Juhanoja, J. Eriksson, M. 2001. Uranium and plutonium containing particles in a sea sediment sample from Thule, Greenland. Journal of Radioanalytical and Nuclear Chemistry 248 (3), 623-627.

[16] Pelowitz, D. 2005. MCNPX™ User's Manual, Version 2.5.0; Los Alamos National Laboratory, Los Alamos, New Mexico, USA.

[17] http://docs.nscl.msu.edu/daq/ (accessed 26.3.2013)

[18] Aarnio, P.A., Ala-Heikkilä, J.J., Isolankila, A., Kuusi, A., Moring, M., Nikkinen, M., Siiskonen, T., Toivonen, H., Ungar, K., Zhang, W. 2008. LINSSI: Database for gamma-ray spectrometry. Journal of Radioanalytical and Nuclear Chemistry 276 (3) 631-637.

[19] Ihantola, S. 2009. Particle locating with the Double Sided Silicon Strip Detector (DSSSD) in PANDA, TTL-TECDOC-2009-035.

[20] CTBTO preparatory commission. 2007. Radionuclide Analysis and Evaluation Software Aatami, software version 4.10, Users Manual.

[21] Toivonen, H., Pelikan, P., Pöllänen, R., Ihantola, S., Ruotsalainen, K. 2010. ADAM - Advanced Deconvolution of Alpha Multiplets, User Manual of Adam 2.8. STUK - Radiation and Nuclear Safety Authority, Helsinki, Finland.

[22] http://www.originlab.com/index.aspx?go=Products/OriginPro (accessed 26.3.2013).

[23] Ihantola, S., Peräjärvi, K., Toivonen, H., Turunen, J. 2010. PANDA analyses methods. TTL-TECDOC-2010-025.

[24] Ihantola, S., 2009. Peak efficiency calibration for the germanium detector in PANDA. TTL-TECDOC-2009-029.

[25] Eriksson, M., Lindahl, P., Roos, P., Dahlgaard, H., Holm, E., 2008. U, Pu, and Am Nuclear Signatures of the Thule Hydrogen Bomb Debris. Environmental Science and Technology 42, 4717-4722.

[26] Lind, O.C., Salbu, B., Janssens, K., Proost, K., Dahlgaard, H., 2005. Characterization of uranium and plutonium containing particles

originating from the nuclear weapons accident in Thule, Greenland, 1968. Journal of Environmental Radioactivity 81, 21-32.

[27] Turunen, J., Ihantola, S., Pöllänen, R. 2011. Tornion ilmanäytteen AT 102/10 mittaus PANDAlla. TTL-TECDOC-2011-009.

[28] Turunen, J., Ihantola, S., Pelikan, A., Peräjärvi, K., Pöllänen, R., Toivonen, H. 2011. Position-sensitive measurement system for non-destructive analysis. Proceedings – Third European IRPA Congress, 14–18 June 2010, Helsinki, Finland. Helsinki: Nordic Society for Radiation Protection; 2011. P12-19, 1974–1979.

[29] Batkin, I., Brun del Re, R., Boutin, J.-G., Armitage, J. 1998. γ-spectroscopy investigation of radon daughter deposition on electrostatically charged surfaces. Physics in Medicine and Biology 43, 487-499.

[30] Knutson, E.O., Gogolak, C.V., Scofield, P., Klemic, G. 1992. Measurements of radon progeny activity on typical indoor surfaces. Radiation Protection Dosimetry 45 (1-4), 313-317.

[31] Pöllänen, R. (ed.) 2003. Säteily –ja ydinturvallisuus 2 - Säteily ympäristössä. Säteilyturvakeskus, Helsinki, ISBN 951-712-995-5.

APPENDIX 1: The decay schemes of ^{239}Pu, ^{240}Pu and ^{241}Am

The schemes are taken from [13].

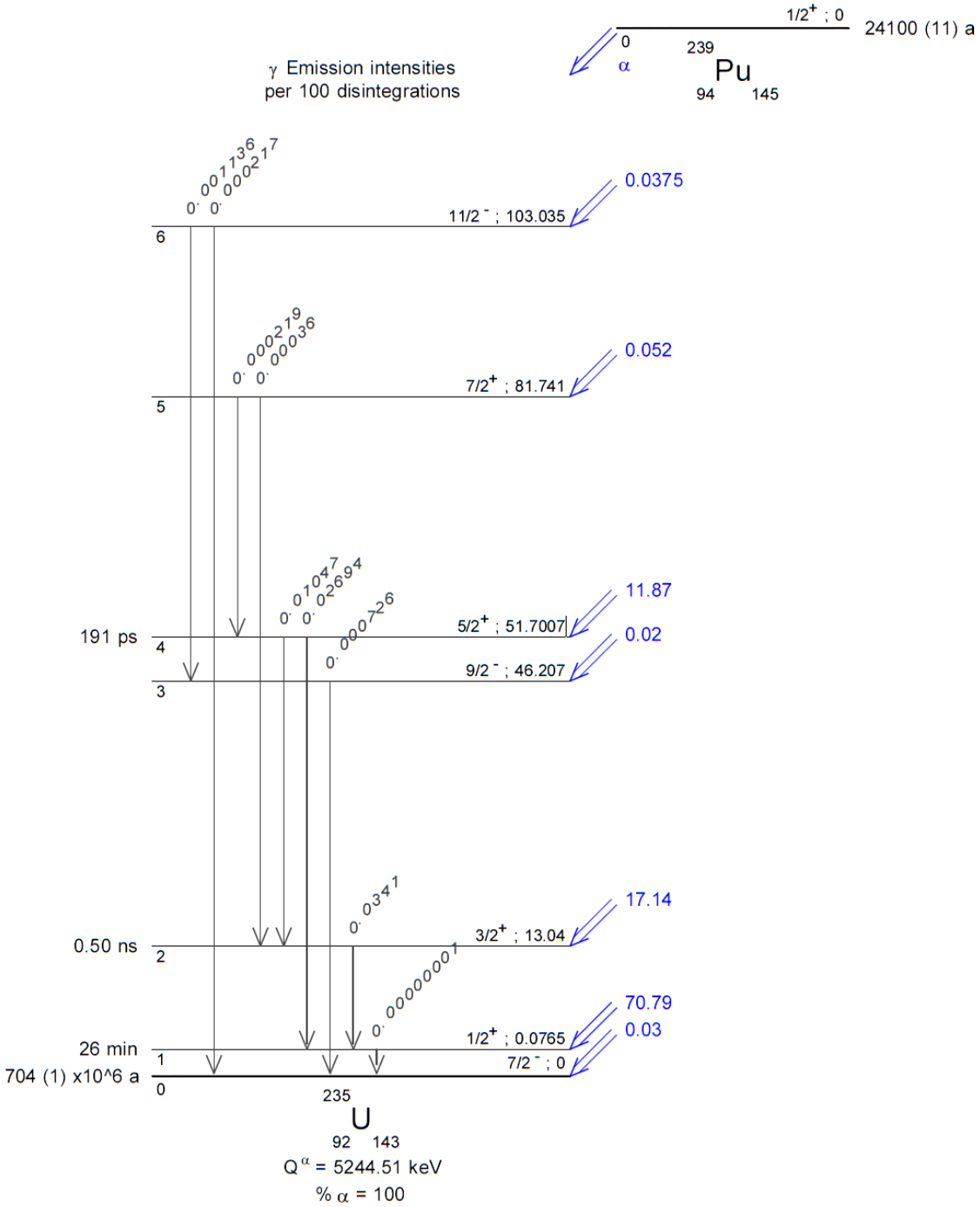

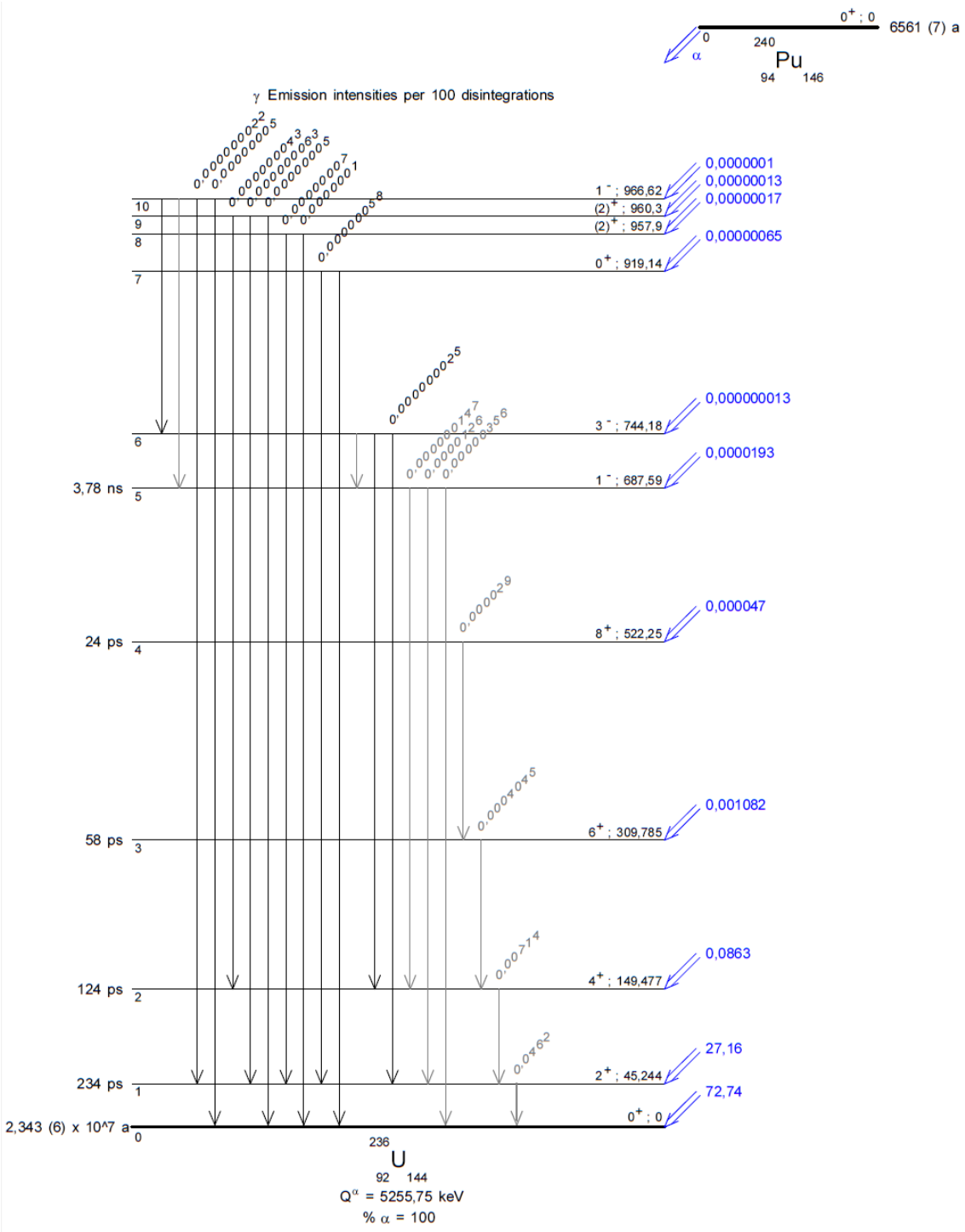
0+ ; 0
6561 (7) a
0
α
240
Pu
94
146
γ Emission intensities per 100 disintegrations
0,0000001
0,00000013
0,00000017
0,00000065
1 - ; 966,62
(2)+ ; 960,3
(2)+ ; 957,9
0+ ; 919,14
10
9
8
7
0,000000025
0,000000147
0,000000126
0,000000356
0,000000013
3 - ; 744,18
6
0,0000193
1 - ; 687,59
3,78 ns
5
0,000029
0,000047
8+ ; 522,25
24 ps
4
0,0004045
0,001082
6+ ; 309,785
58 ps
3
0,007114
0,0863
4+ ; 149,477
124 ps
2
0,04762
27,16
2+ ; 45,244
234 ps
1
72,74
0+ ; 0
2,343 (6) x 10^7 a
0
236
U
92
144
Qα = 5255,75 keV
% α = 100

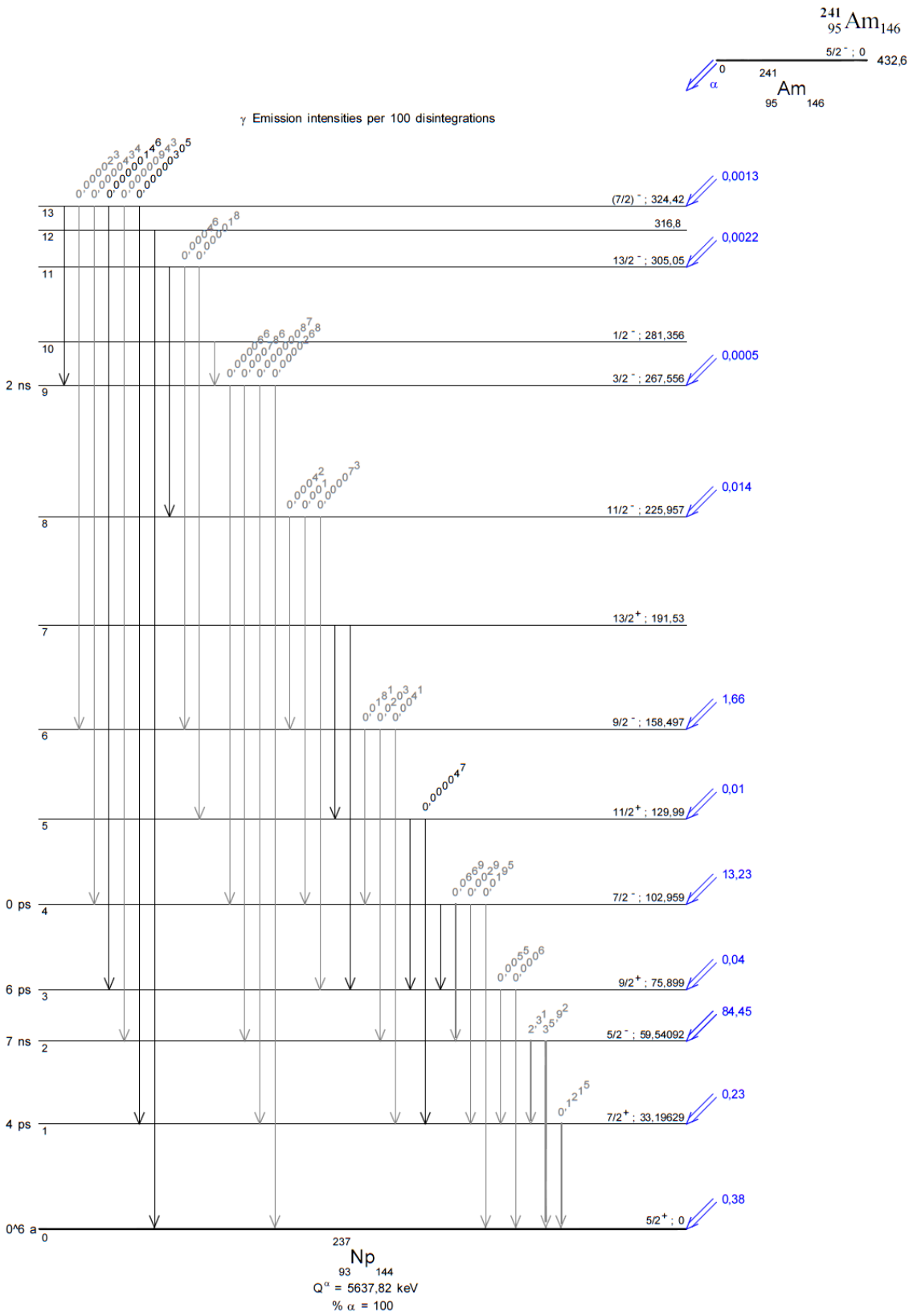
241 95 Am 146
5/2⁻ ; 0
432,6
0
α
241
Am
95 146
γ Emission intensities per 100 disintegrations
0,0013
(7/2)⁻ ; 324,42
316,8
0,0022
13/2⁻ ; 305,05
1/2⁻ ; 281,356
0,0005
3/2⁻ ; 267,556
2 ns
0,014
11/2⁻ ; 225,957
13/2⁺ ; 191,53
1,66
9/2⁻ ; 158,497
0,01
11/2⁺ ; 129,99
13,23
7/2⁻ ; 102,959
0 ps
0,04
9/2⁺ ; 75,899
6 ps
84,45
5/2⁻ ; 59,54092
7 ns
0,23
7/2⁺ ; 33,19629
4 ps
0,38
5/2⁺ ; 0
0^6 a
237
Np
93 144
Q^α = 5637,82 keV
% α = 100

APPENDIX 2: Naturally occurring decay chains

The figure is taken from [31].